Dynamic glucose uptake, storage, and release by human microvascular endothelial cells

Samaneh Yazdani[a], Philip J. Bilan[a], Javier R. Jaldin-Fincati[a,†], Janice Pang[a], Felicia Ceban[a], Ekambir Saran[a], John H. Brumell[a,b,c,d], Spencer A. Freeman[a,e,*], and Amira Klip[a,e,f,g,*]

[a]Cell Biology Program, The Hospital for Sick Children, Toronto, ON, Canada, M5G 0A4; [b]Department of Molecular Genetics, [c]Institute of Medical Science, [e]Department of Biochemistry, [f]Department of Paediatrics, and [g]Department of Physiology, University of Toronto, Toronto, ON, Canada, M5S 1A1; [d]SickKids IBD Centre, Hospital for Sick Children, Toronto, ON, Canada, M5G 0A4

ABSTRACT **Endothelia determine blood-to-tissue solute delivery, yet glucose transit is poorly understood. To illuminate mechanisms, we tracked [^{3}H]-2-deoxyglucose (2-DG) in human adipose-tissue microvascular endothelial cells. 2-DG uptake was largely facilitated by the glucose transporters GLUT1 and GLUT3. Once in the cytosol, >80% of 2-DG became phosphorylated and ~20% incorporated into glycogen, suggesting that transported glucose is readily accessible to cytosolic enzymes. Interestingly, a fraction of intracellular 2-DG was released over time (15–20% over 30 min) with slower kinetics than for uptake, involving GLUT3. In contrast to intracellular 2-DG, the released 2-DG was largely unphosphorylated. Glucose release involved endoplasmic reticulum–resident translocases/phosphatases and was stimulated by adrenaline, consistent with participation of glycogenolysis and glucose dephosphorylation. Surprisingly, the fluorescent glucose derivative 2-NBD-glucose (2-NBDG) entered cells largely via fluid phase endocytosis and exited by recycling. 2-NBDG uptake was insensitive to GLUT1/GLUT3 inhibition, suggesting poor influx across membranes. 2-NBDG recycling, but not 2-DG efflux, was sensitive to N-ethyl maleimide. In sum, by utilizing radioactive and fluorescent glucose derivatives, we identified two parallel routes of entry: uptake into the cytosol through dedicated glucose transporters and endocytosis. This reveals the complex glucose handling by endothelial cells that may contribute to glucose delivery to tissues.**

Monitoring Editor
Michael Marks
Children's Hospital of Philadelphia

Received: May 2, 2022
Revised: Jul 14, 2022
Accepted: Jul 26, 2022

INTRODUCTION

The vascular endothelium network coordinates nutrient transport between the circulation and tissues and has an important function in the control of energy balance (Huang *et al.*, 2012; Rohlenova *et al.*, 2018). In the brain, muscles, and adipose tissues, microvascular endothelial cells form tight junctions that impart a level of resistance to paracellular transport. Many macromolecules are therefore transported across the cells (Yazdani *et al.*, 2019). This transcellular route of delivery has been exploited to deliver therapeutics into the interstitial brain milieu. However, how small molecules and nutrients in particular traverse microvessels toward the parenchyma is less documented, yet it is paramount to the survival of these tissues.

Glucose, an essential energy substrate, travels in the blood and must traverse the capillary endothelia to supply parenchymal cells. Strikingly, the metabolic handling of glucose by microvascular

This article was published online ahead of print in MBoC in Press (http://www.molbiolcell.org/cgi/doi/10.1091/mbc.E22-04-0146) on August 3, 2022.

Author contributions: A.K. managed the project; S.A.F. and A.K. conceived experiments; S.A.F. conceived analysis; J.H.B. contributed advice and discussion; S.Y., P.J.B., J.R.J-F., J.P.,F.C., E.S., and S.A.F performed experiments; S.Y., P.J.B., J.R.J-F., J.B., and F.C. performed analysis; P.J.B. and A.K. drafted the manuscript; S.A.F. edited the manuscript; A.K. acts as a guarantor.

Competing financial interests: The authors declare no competing financial interests.

†Present address: Unidad de Conocimiento Traslacional Hospitalaria E. Paz Chain 30, CP 4400, Salta, Argentina.

*Address correspondence to: Amira Klip (amira@sickkids.ca); Spencer A. Freeman (spencer.freeman@sickkids.ca).

Abbreviations used: CB, cytochalasin B; DEAE-FF, diethylaminoethyl-fast flow sepharose; 2-DG, 2-deoxyglucose; ER, endoplasmic reticulum; G6Pase, glucose-6-phosphatase; G6PT, glucose-6-phosphate translocase; GLUT, glucose transporter (SLC2A family); HAMEC, human adipose-tissue derived endothelial cells; Hx, hexokinase; 2-NBDG, 2-(N-[7-nitrobenz-2-oxa-1, 3-diazol 4-yl] amino)-2-deoxyglucose; NEM, N-ethyl maleimide; NSF, NSF-sensitive factor; PGM, phosphoglucomutase; SRB, sulforhodamine B; UGPP, UDP-glucose pyrophosphorylase; WGA, wheat germ agglutinin.

endothelial cells is not well understood (Rohlenova *et al.*, 2018). According to the most popular view, glucose in the circulation is transported into and out of endothelial cells via Glucose Transporter 1 (GLUT1; Goldstein *et al.*, 1977; Betz *et al.*, 1979; Patching, 2017; Szablewski, 2017; Willemsen *et al.*, 2017; Yazdani *et al.*, 2019). This paradigm is confirmed by the low cerebrospinal glucose levels observed in GLUT1 Deficiency Syndrome (De Vivo *et al.*, 1991). To be effective, however, this delivery route would require the incoming glucose to circumvent metabolic utilization by the endothelial cell. Moreover, GLUT1 has been observed to be enriched luminally, that is, facing the flow of blood (Koepsell, 2020), which would limit its capacity to efflux glucose to the underlying interstitium. The metabolism of glucose is also essential for microvascular integrity and angiogenesis (De Bock *et al.*, 2013; Rohlenova *et al.*, 2018; Veys *et al.*, 2020), prompting the question: Whether and how can a fraction of endothelial cell–associated glucose be spared from its consumption to remain available for release? Additionally, it raises the possibility that glucose may enter the cells through routes that prevent it from reaching cytosolically located glycolytic enzymes. Metabolic rerouting, vesicular and paracellular transit delivery emerge as possibilities but have not been previously investigated.

Here, we endeavor to investigate how glucose derivatives are internalized by primary human adipose tissue–derived microvascular endothelial cells (HAMEC). By analyzing the uptake of radioactive glucose derivatives and tracking fluorescence glucose derivatives in live cells, we identified two parallel routes of entry: uptake into the cytosol through dedicated glucose transporters and robust endocytosis. Uptake of the glucose derivative [^{3}H]-2-deoxyglucose ([^{3}H]-2-DG) occurred largely through facilitative glucose transporters (primarily GLUT1 and GLUT3) and underwent both phosphorylation and partial incorporation into glycogen. Internalized 2-DG also exited cells, but only in a non-phosphorylated form. This exit was mediated in part via GLUT3. In contrast, the fluorescent glucose derivative 2-NBD-glucose (2-NBDG) was not transported via GLUTs 1/3 and was instead trapped in the endocytic pathway where it was rapidly released from the cells through endosomal recycling pathways.

Together, these new findings are of relevance to our understanding of glucose delivery to tissues, as both the cytosolic and endocytic routes of glucose entry must be considered. The radioactive 2-DG allowed us to quantify the transport, metabolic processing and release of glucose, whereas the fluorescent 2-NBDG allowed us to identify the endocytic route, explaining an ongoing controversy on its mechanism of entry.

RESULTS

Human adipose tissue–derived microvascular endothelial cell take-up of [^{3}H]-2-deoxyglucose via GLUT1 and GLUT3

We recently established that HAMEC retain properties of their niche and are a useful system for studying macromolecule uptake (Azizi *et al.*, 2015; Jaldin-Fincati *et al.*, 2018). Accordingly, we selected this system to study glucose handling by microvascular endothelia, in a cellularly amenable manner.

Glucose is a primary nutrient of most cells and requires dedicated transporters to reach the cytosol for metabolic processing. The downward gradient for glucose is dictated by its rapid metabolism, such that most cells have minimal or undetectable levels of free glucose. To study glucose entry routes and kinetics, it has been customary to use glucose derivatives that cannot undergo metabolism. The most widely used derivative is [^{3}H]-2-deoxyglucose ([^{3}H]-2-DG), which has been validated as a *bona fide* substrate of glucose transporters of the SLC2A family (comprising GLUTs 1-14; Mueckler and Thorens, 2013). Once inside mammalian cells, [^{3}H]-2-DG is readily phosphorylated at C-6 by hexokinases, but it cannot proceed further through glycolysis as it cannot undergo conversion to fructose-6-phosphate (Horton *et al.*, 1973).

Endothelial and epithelial cells present a unique challenge in the handling of glucose: their cellular constituents require glucose for energy procurement but also need to deliver glucose to the parenchymal cells facing their basolateral surfaces. Thus, mechanisms for glucose to evade catabolism across these barriers should exist. Uptake of 50 μM [^{3}H]-2-DG was linear in time for up to 60 min (Figure 1A). When measured at 30 min, [^{3}H]-2-DG uptake was competed for by ~40% with either 1 mM 2-DG or 1 mM glucose (Figure 1B), attesting to its uptake via facilitated mechanisms.

BAY-876 ([N^4-[1-(4-cyanobenzyl)-5-methyl-3-(trifluoromethyl)-1H-pyrazol-4-yl]-7-fluoroquinoline-2,4-dicarboxamide]) is a hexose uptake inhibitor with high affinity for GLUT1 (IC_{50} of 2 nM) and a >130-fold lower affinity for GLUTs 2, 3 or 4, the IC_{50} of BAY-876 for GLUT3 being 1.67 μM (Siebeneicher *et al.*, 2016). Uptake of [^{3}H]-2-DG for 30 min into HAMEC was sensitive to BAY-876 in the nM range, to a maximum of only 50% (Figure 1C). Uptake was further inhibited at micromolar doses of BAY-876 approaching a maximum inhibition of 85% at 20 μM (Figure 1D). These results are consistent with GLUT1 mediating approximately half of the facilitated uptake of [^{3}H]-2-DG into HAMEC, with the remainder being mediated by other GLUT family members, based on its inhibition by 20 μM BAY-876 and substantial competition by 10 mM glucose (Figure 1E). The notion that glucose is taken into HAMEC by GLUTs is supported by experiments demonstrating that pretreatment of the monolayers with 10 μM cytochalasin B, which has an IC_{50} of ~ 0.4 μM for GLUTs 1 and 3, completely ablated [^{3}H]-2-DG uptake (Figure 1E). This is in line with the partial reduction in 2-DG uptake into human umbilical vein endothelial cells depleted of GLUT1 and/or GLUT3 (Tumova *et al.*, 2016).

Of the 12 GLUT family members, HAMEC indeed express transcripts of GLUT1 and GLUT3 in high abundance and, to a lesser extent, GLUTs 6 and 10 (Figure 1F). We detected virtually no expression of the other GLUT family members nor of Na^+-glucose–linked transporters (SGLT1 and SGLT2; Figure 1F). HAMEC also express readily detectable levels of GLUT1 and GLUT3 protein as detected by immunoblotting (Figure 1G). Prominence of GLUT1 and GLUT3 is common to other endothelial cells (Knott *et al.*, 1996), suggesting these transporters could play ubiquitous roles throughout the vasculature. Taken together, these findings suggest that [^{3}H]-2-DG enters HAMEC through GLUT1 and GLUT3.

Of note, it is customary and advisable to use micromolar levels of [^{3}H]-2-DG to measure initial rates of uptake through the transporters properly and assess its regulation, rather than measuring [^{3}H]-2-DG uptake in the presence of the physiological glucose concentration (5 mM), which is three- to fivefold higher than the K_m of GLUT1 and GLUT3. Nonetheless, in a separate experiment, we compared the uptake of tracer [^{3}H]-2-DG for 30 min in media containing 5 mM glucose with that in zero glucose media containing only 50 μM 2-DG plus tracer [^{3}H]-2-DG. While, as expected, the dpm [^{3}H]-2-DG taken up were much lower in 5 mM glucose than in glucose-free media containing only 50 μM [^{3}H]-2-DG, the net uptake of hexose entering the cells (based on the specific activity of [^{3}H]-2-DG considering the 5 mM glucose) amounted to 15.9 ± 1.8 nmol/min/mg protein compared with 0.61 ± 0.12 nmol/min/mg protein for uptake in zero glucose media (mean ± SEM). These results attest to the capacity of HAMEC to take up glucose.

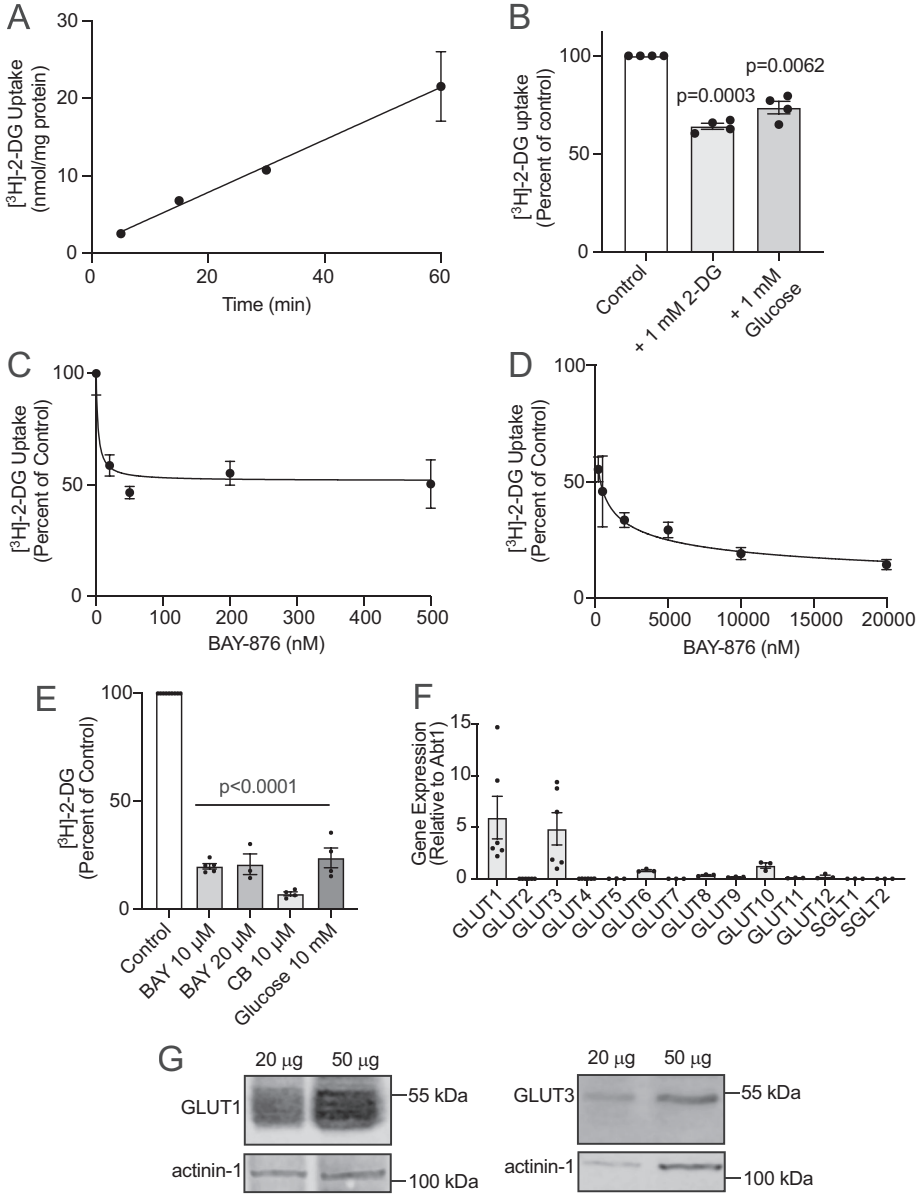

FIGURE 1: GLUT1 and GLUT3 facilitate 2-deoxyglucose uptake in HAMEC. For uptake, HAMEC grown in 12-well plates were rinsed with PBS (with Ca^{2+} and Mg^{2+}) and then incubated with glucose-free DMEM supplemented with [^{3}H]-2-DG (1 µCi/ml, 50 µM). In (A) uptake times were 5, 15, 30, and 60 min at 37°C. The cells were washed with ice-cold saline to stop uptake and lysed with 0.05 M NaOH. Lysates were prepared for scintillation counting and protein determination. Results are presented as the mean ± SEM nmol/mg protein from four independent experiments performed in triplicate per condition ($p = 0.0012$, 5 vs. 30 min and $p < 0.0001$, 5 vs. 60 min, one-way ANOVA—*Note*: Error bars for the 5-, 15-, and 30-min timepoints are smaller than the symbols). (B) [^{3}H]-2-DG uptake was performed for 30 min in the presence of 1 mM of 2-DG or D-glucose. Results are the mean ± SEM percent of control uptake without added hexose (set to 100%) from four experiments, in duplicate (indicated *p*-values vs. control). (C, D) [^{3}H]-2-DG uptake was performed for 30 min with the indicated concentrations of BAY-876 (vehicle 0.1% vol/vol DMSO). Results are the mean ± SEM percent of control uptake. Dose–response plots illustrate the results for the 0 to 500 nM, C, and 200 nM to 20 µM, D, BAY-876 conditions performed in duplicate across two to seven independent experiments, in duplicate, for each condition. Results are the mean ± SD percent of control uptake ($p < 0.05$ for 200 and 500 nM BAY-876 *vs* control and $p < 0.001$ BAY-876 for 2–20 µM vs. control). (E) [^{3}H]-2-DG uptake was performed for 30 min with the indicated concentration of inhibitor BAY-876 (10 or 20 µM, BAY), cytochalasin B (10 µM, CB), high glucose (10 mM) compared with control (0.1% vol/vol DMSO; n = three to five independent experiments, in duplicate, per condition ($p < 0.0001$ for all conditions vs. control, one-way ANOVA). (F) qPCR analysis (in duplicate from three or six experiments) for mRNA expression of 12 members of facilitative glucose transporters (GLUTs, SLC2A gene family) and the sodium–glucose transporters SGLT1 or SGLT2 (SLC5A gene family) using the $\Delta\Delta C_T$ method compared with the ABT1 reference gene (*p*-value is 0.0004 for all conditions, one-way ANOVA). (G) HAMEC protein lysates were processed for immunoblotting for GLUT1 and GLUT3. Shown are representative immunoblots of at least three independent experiments. Relative molecular weight markers indicated.

Human adipose tissue–derived microvascular endothelial cells export glucose to the medium, partially utilizing GLUT3

We next enquired whether HAMEC can export glucose by measuring radioactivity release following a 30 min pulse of [^{3}H]-2-DG. Chase periods of up to 90 min revealed a steady release of the [^{3}H]-2-DG radioactivity captured by HAMEC (Figure 2A), amounting to at least 20% of the total cellular content at 30 min of chase time (Figure 2, B–D). Notably, and in contrast to the marked inhibition of [^{3}H]-2-DG uptake by BAY-876, the efflux of [^{3}H]-2-DG was insensitive to submicromolar doses of the compound but was reduced by half with 20 µM BAY-876 (Figure 2C). Similarly, 10 µM cytochalasin B also inhibited only ~50% of [^{3}H]-2-DG released from cells (Figure 2D), indicating that a parallel route, that is, one distinct from GLUTs, must also mediate its release. These results are consistent with a partial contribution of GLUT3 and a very minor role for GLUT1 in [^{3}H]-2-DG exit from cells.

When the [^{3}H]-2-DG pulse (30 min) was performed in media containing 5 mM glucose, the rate of efflux measured at 30 min of chase was 2.61 ± 0.20 nmol/min/mg protein, compared with 0.098 ± 0.007 nmol/min/mg protein in glucose-free media (mean ± SEM). Therefore, the mass of glucose released was 26.6 times higher in 5 mM glucose, but still represented about 16 to 17% of the glucose content inside the cells. These results strongly suggest that the higher amount of glucose entering the cells created a larger pool available for efflux.

To complement the above findings, we investigated the localization of GLUT1 and GLUT3 in HAMEC (Supplemental Figure 1). Because antibodies to GLUT3 are not reliable for immunofluorescence, we instead generated tagged versions of GLUT1 and GLUT3. Specifically, we generated GLUT1 and GLUT3 plasmids containing a modified haloalkane dehalogenase (HaloTag). Once expressed in cells, these tagged transporters were illuminated with a chloroalkane linker conjugated with a fluorescent dye

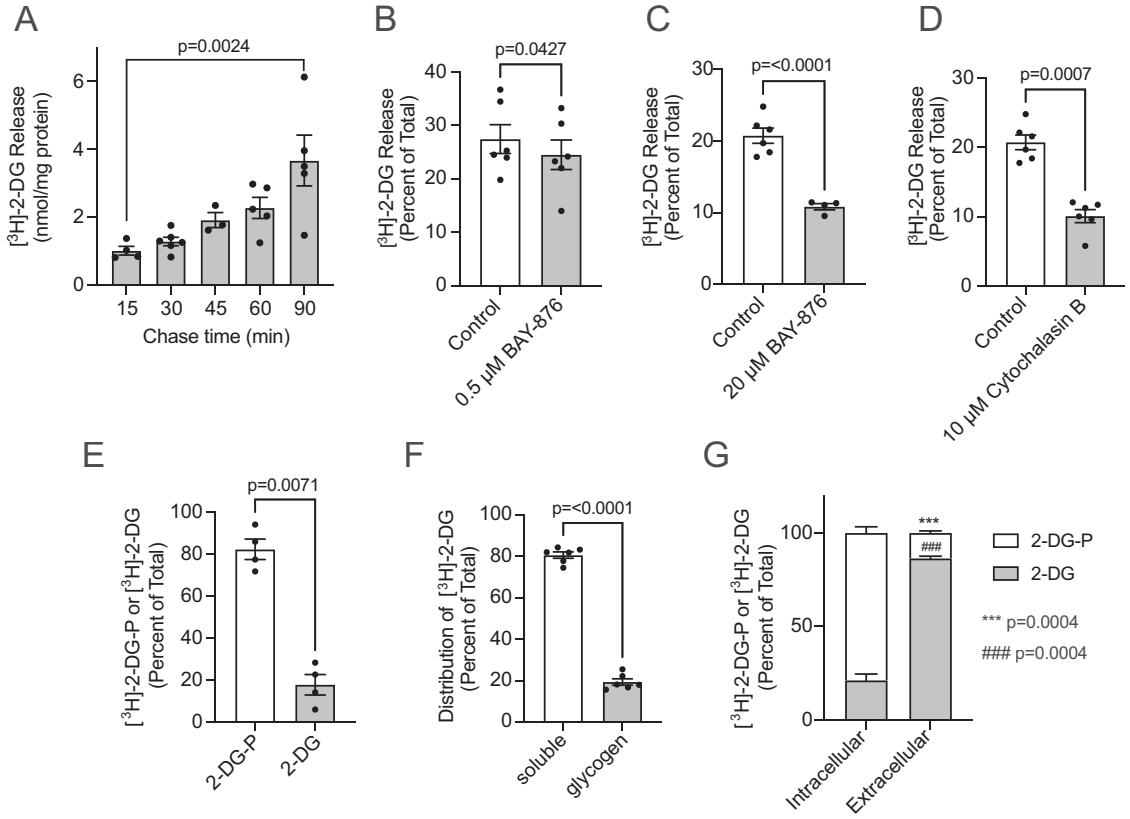

FIGURE 2: Internalized glucose does not exit via GLUT1 in HAMEC. HAMEC cells grown in 12-well plates were rinsed with PBS pulsed with [^{3}H]-2-DG (2 μCi/ml 50 μM, 30 min, 37°C) in glucose- and serum-free DMEM. The cells were rinsed three times with PBS and chased in 0.5 ml/well DMEM (with 5 mM glucose) + 10% FBS. (A) Radioactivity released from the cells for 15, 30-, 45-, 60-, and 90-min chase times. Illustrated are the mean [^{3}H]-counts ± SEM (nmol/mg lysate protein minus background counts at 0 min) relative to cell-associated [^{3}H]-counts in no-chase cells (n = 3 or 6, indicated p-value 15 min vs. 90 min, one-way ANOVA). (B–D) HAMEC cells were pulsed with [^{3}H]-2-DG and chased for 30 min including 0.1% vol/vol DMSO (control), (B) 0.5 μM BAY-876, (C) 20 μM BAY-876, or (D) 10 μM cytochalasin B. Results expressed as the mean ± SEM (n = 4 or 6 experiments, duplicate conditions; indicated p-value vs. control, Student's paired t test, two-tailed). (E) HAMEC were grown in six-well plates and pulsed with 1.0 ml of [^{3}H]-2-DG (2 μCi/ml 50 μM, 30 min, 37°C) as in A. Media were discarded and cells were quickly rinsed with ice-cold PBS and immediately lysed in 50% ethanol. Lysates were clarified by centrifugation and loaded on DEAE-FF anion exchanger columns to separate samples into nonphosphorylated or phosphorylated [^{3}H]-2-DG fractions, as detailed in *Materials and Methods*. Data represent the nonphosphorylated or phosphorylated [^{3}H]-2-DG and were plotted as the mean ± SEM percentage of the sum total of cell-associated [^{3}H]-counts (n = 4 independent experiments, indicated p-value for 2-DG-P *vs* 2-DG, Student's paired t test, two-tailed). (F) HAMEC were pulsed with [^{3}H]-2-DG (2 μCi/ml 50 μM, 30 min, 37°C). Cells were lysed and glycogen was pelleted from soluble cell components as detailed in *Materials and Methods*. Distribution of the radioactivity between the soluble cell fractions and glycogen are the mean ± SEM percent of total cell counts (n = 6 independent experiments, $p < 0.0001$, soluble vs. glycogen, Student's paired t test, two-tailed). (G) HAMEC were pulsed with [^{3}H]-2-DG as in E. This was followed by 30 min chase at 37°C. Media and 50% ethanol cell lysates were collected and prepared for DEAE-FF column fractionation and scintillation counting as in F. Data representing nonphosphorylated or phosphorylated [^{3}H]-2-DG from cell lysates (Intracellular) or from media (Extracellular) were plotted as percentages of their respective total cell-associated [^{3}H]-counts (n = 4 independent experiments, indicated p-values for 2-DG-P vs. 2-DG in intracellular or extracellular samples, Student's paired t test, two-tailed).

(HaloTag ligand; Los *et al.*, 2008). Halo-GLUT1 localized to the plasma membrane and to endomembranes, whereas Halo-GLUT3 was more circumscribed to surface membranes (Supplemental Figure 1). Neither GLUT1 nor GLUT3 grossly showed preferential targeting between the apical and basolateral membranes of HAMEC cells in monolayers. While acknowledging the overexpressed levels, these results suggest that both transporters could be positioned to allow glucose transfer into the cell and potentially out of the cell. The endomembrane distribution of GLUT1 also suggests that it may dynamically recycle to the plasma membrane and/or distribute more stably to an endosomal population.

The above findings prompted an examination of the intracellular processing of [^{3}H]-2-DG. Analysis of the radioactivity taken up by HAMEC in 30 min showed that the vast majority was phosphorylated, consistent with robust action of hexokinases on the glucose derivative (Figure 2E). In separate experiments, we compared in parallel the proportion of phosphorylated to unphosphorylated glucose inside HAMEC when the uptake pulse containing tracer [^{3}H]-2-DG was supplemented with 5 mM glucose or when it contained only 50 μM 2-DG plus the tracer [^{3}H]-2-DG. In these experiments the proportion of phosphorylated hexose upon uptake of 50 μM 2-DG plus the tracer was even higher than before (90.5 ± 2.2%), and in the

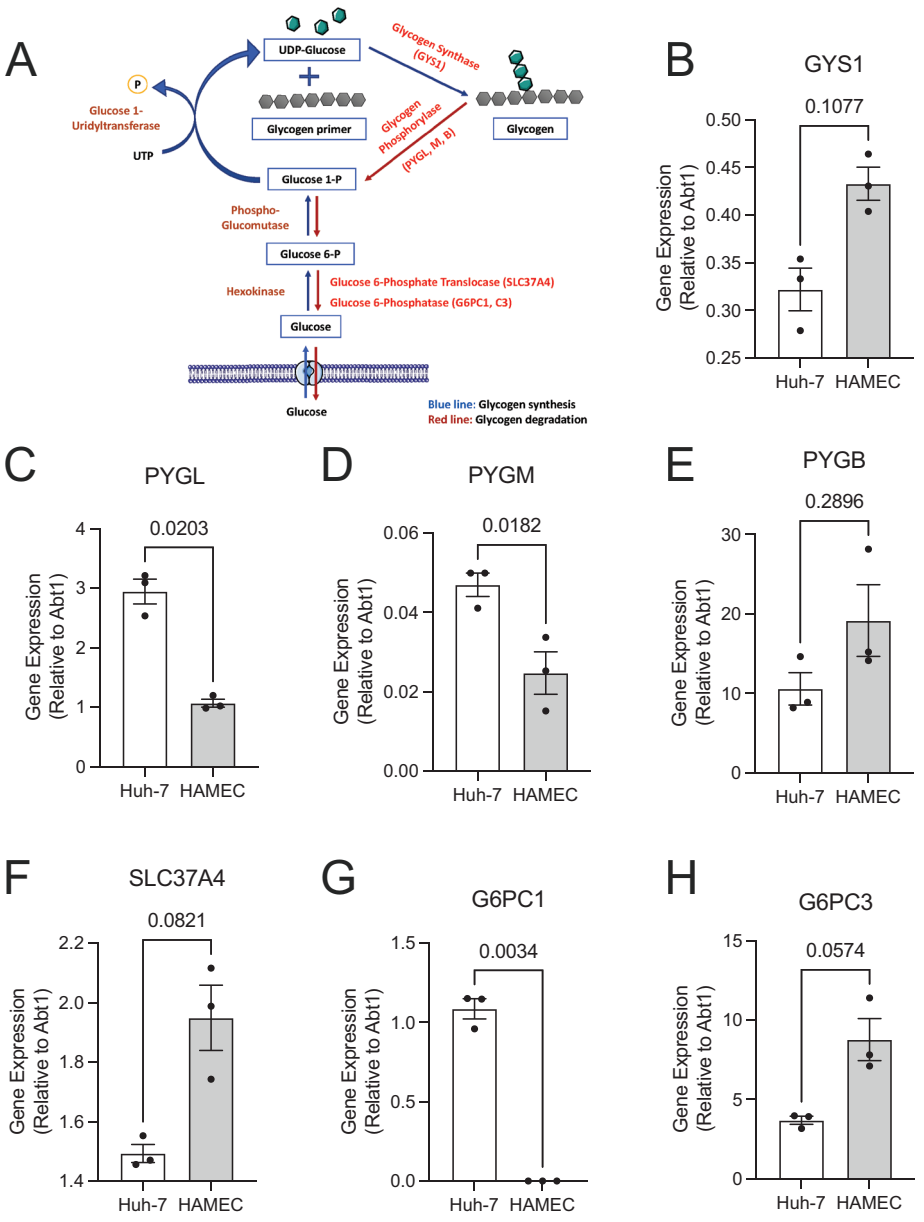

FIGURE 3: HAMEC express key glycogen metabolism enzymes. (A) Shown is a schematic metabolic pathway outlining the synthesis (blue arrows) and breakdown (red arrows) of glycogen. (B–H) Expression of enzymes indicated in red font, A were quantified in human Huh-7 liver cells or HAMEC by qPCR with TaqMan probes using the $\Delta\Delta C_t$ method compared with the ABT1 reference gene ($n = 3$ experiments, in duplicate, indicated p-values calculated using Student's paired t test, two-tailed). Shown are the relative mean ± SEM mRNA expression for GYS1, B; PYGL, C; PYGM, D; PYGB, E; SLC37A4, F; G6PC1, G; and G6PC3, H. GYS = glycogen synthase, PYG = glycogen phosphorylase (liver brain, muscle isoforms: L, B, M), SLC37A4 = glucose-6-phosphate translocase, G6PC = glucose-6-phosphate phosphatase catalytic subunit.

into glycogen, a process that can be substantial in skeletal and cardiac muscles in vivo (Virkamaki *et al.*, 1997), hepatoma cells (Nigam, 1967), and liver homogenates (Nigam and Fridland, 1967).

The considerable phosphorylation of [^{3}H]-2-DG within HAMEC and the incorporation of the remainder into glycogen highlight its accessibility to cytosolic enzymes, consistent with the majority of [^{3}H]-2-DG uptake occurring through facilitated transporters. Indeed, along with enzymes mediating glycogen synthesis (e.g., glycogen synthase1: GYS1, Figure 3B) HAMEC express those involved in glycogenolysis (liver-type glycogen phosphorylase: PYGL; myophosphorylase: PYGM; and glycogen phosphorylase B: PYGB; Figure 3, C–E). Their expression is compared with that in the human liver cell line Huh7 (both relative to a housekeeping gene) and reveals a high expression of phosphorylase in HAMEC. Notably, HAMEC also express higher levels of glucose-6-phosphate translocase (SLC37A4) and of the nonhepatic isoform of glucose-6-phosphatase catalytic subunit (G6PC3; Figure 3, F and H). These determinations strongly support the ability of HAMEC to enact glycogen synthesis, glycogenolysis, and importantly dephosphorylation of glucose-6-phosphate to yield free glucose in the endoplasmic reticulum (ER). This is inferred from the known localization of SLC37A4 and G6PC3 to the ER membrane (Vorhaben and Campbell, 1979; van Schaftingen and Gerin, 2002), where, at least in hepatocytes, they translocate glucose-6-phosphate and hydrolyze the phosphate bond to release the free glucose to the ER lumen.

Human adipose tissue–derived microvascular endothelial cells release [^{3}H]-2-DG through a process involving glycogenolysis and glucose dephosphorylation

In contrast to the high level of phosphorylation of [^{3}H]-2-DG within HAMEC, the released fraction was found to be predominantly unphosphorylated (Figure 2G). In additional experiments, the proportion of unphosphorylated hexose released to the media collected during the chase period did not differ when the loading [^{3}H]-2-DG pulse contained 5 mM glucose (6.1 ± 0.9% of total hexose released) compared with loading in zero-glucose media (7.4 ± 1.4%). These findings raised the possibility that intracellular phosphorylated [^{3}H]-2-DG may undergo dephosphorylation before exiting the cell. This is consistent with these cells exhibiting high expression of G6PC3, a nonhepatic isoform of the glucose-6-phosphatase enzymatic complex (Figure 3H). Alternatively, only the unphosphorylated 15–20% present in the cells might be amenable for efflux. To address these concepts, we assessed how regulation of intracellular glucose pools would impact on glucose efflux in live cells.

presence of 5 mM glucose it was still predominating (81.8 ± 6.8%). This illustrates the high capacity of hexokinase and phosphoglucomutase activities in HAMEC.

The presence of <20% of unphosphorylated intracellular hexose suggested either its metabolic processing into other metabolites or its escape from hexokinase access. Consistent with metabolic processing, ~15 to 20% of the intracellular [^{3}H]-2-DG radioactivity was found associated with the purified glycogen fraction (Figure 2F). This is reminiscent of reports that [^{3}H]-2-DG can indeed incorporate

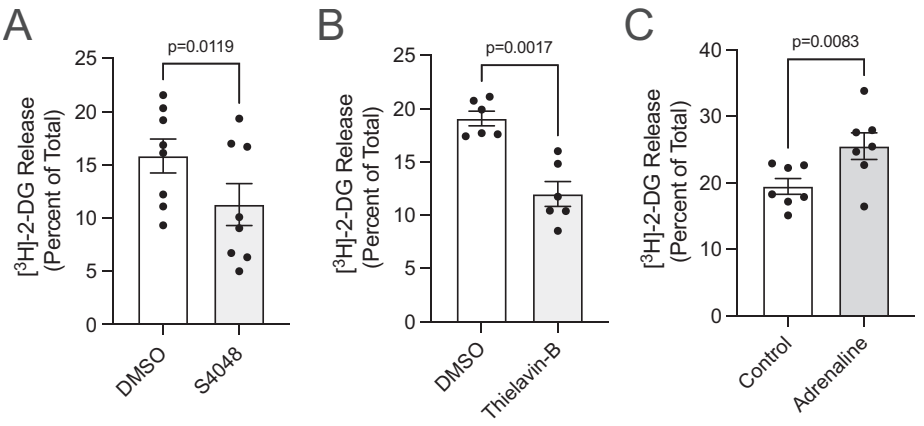

FIGURE 4: A proportion of glucose release follows a canonical glucose-6-phosphate translocase and glucose-6-phosphate-phosphatase route. HAMEC were pulsed with [^{3}H]-2-DG as in Figure 2. This was followed by 30-min (A and B) or 15-min (C) chase periods at 37°C that included (A) 10 μM glucose-6-phosphate translocase inhibitor, S4048 vs. control (0.1% vol/vol DMSO); (B) 100 μM glucose-6-phosphatase inhibitor, Thielavin B vs. control (1% vol/vol DMSO); (C) 1 μM adrenaline vs. no-addition control. Results are the percent [^{3}H]-counts released from the cells after 30- or 15-min chase periods relative to cell-associated [^{3}H]-counts in no-chase cells. (A) n = 8; (B) n = 6; and (C) n = 7 independent experiments, indicated p-values calculated with Student's paired t test, two-tailed.

As illustrated above, over 80% of intracellular [^{3}H]-2-DG is phosphorylated, with ~20% remaining unphosphorylated and a similar amount copurifying with glycogen (Figure 2, E and F). We also determined that ~15 to 20% of the intracellular [^{3}H]-2-DG is released after just 30 min of chase and continues to exit over longer periods of time (Figure 2A). We reasoned that, if glycogenolysis contributed to release from the cells of unphosphorylated glucose, its conversion into glucose-6-phosphate would be a prerequisite. To approach the scenario in which the activity of a glucose-6-phosphatase is required for glucose release, we inhibited the glucose-6-phosphate translocase or glucose-6-phosphatase activities at the ER membrane. The chlorogenic acid analogue S4048 is a reported inhibitor of the glucose-6-phosphate translocase (Bandsma *et al.*, 2001; Gustafson *et al.*, 2001) and Thielavin-B is an inhibitor of the glucose-6-phosphatase activity (Sakemi *et al.*, 2002). Both compounds significantly reduced the release of [^{3}H]-2-DG in the pulse and chase paradigm (Figure 4, A and B). These findings uncover a previously unrealized utilization of the mechanism of glucose-6-phosphate dephosphorylation in the process of glucose release from endothelial cells.

Storage of glucose as glycogen and release through the ER would afford protection from glycolytic utilization, essentially constituting a storage strategy for glucose destined for release. The chemical measurement of glycogen yielded 0.18 μg glycogen/μg protein in HAMEC, in a similar range present in human hepatoma Huh7 cells (0.5 μg glycogen/μg protein). These tantalizing observations raise the possibility that glycogen is a source for the eventually exported glucose, as is the case in the liver but is not typical of any other tissue of the body.

Accordingly, we explored if promoting glycogenolysis would increase glucose release. HAMEC were treated with adrenaline exclusively during the chase period in cells pulsed with [^{3}H]-2-DG. Notably, adrenaline caused statistically significant stimulation of release (Figure 4C), despite the very short time of action. This finding exposes the possibility for physiological regulation of glucose storage and release by endothelial cells, which may play a significant role in rendering glucose to surrounding tissues in vivo.

Subcellular localization of fluorescent glucose derivatives

To locate glucose intracellularly, we visualized the distribution of the fluorescent glucose derivatives. 2-(N-[7-nitrobenz-2-oxa-1, 3-diazol 4-yl] amino)-2-deoxyglucose (2-NBDG), a fluorescent D-glucose derivative that has been employed to score glucose influx into live mammalian cells (Yamada *et al.*, 2007). For the most part, however, 2-NBDG has not been used in imaging studies to determine its intracellular localization. Like 2-DG, 2-NBDG can be phosphorylated by hexokinases at C-6 but cannot progress to glycolysis (Yoshioka *et al.*, 1996b; Yamada *et al.*, 2000).

Given the endosomal distribution of GLUT1 and to a lesser degree of GLUT3 shown in Supplemental Figure 1, we opted to pulse HAMEC with 2-NBDG along with the fluid phase marker Sulforhodamine B (SRB), a bright photostable fluorophore of a similar size, as a control. Unexpectedly, 2-NBDG presented with a punctate appearance when imaged after a 15-min uptake pulse (Figure 5A). The related 6-NBDG, which cannot be phosphorylated by hexokinases given its fluorophore labelling at position C-6, followed a similar pattern (unpublished data). The location of the 2-NBDG puncta coincided markedly with that of the internalized SRB, resulting in a high coefficient of colocalization determined using Pearson's analysis (Figure 5A). These data suggest that both dyes were taken up efficiently via endocytosis. Reinforcing this possibility, we detected the intracellular location of the SRB puncta after 1-min, 5-min or 15-min uptake pulses, along with the plasma membrane illuminated by fluorescently tagged wheat germ agglutinin (WGA; Supplemental Figure 2A). Moreover, the dynamic membrane dye FM4-64, which intercalates into the plasma membrane and remains membrane-associated during endocytosis, revealed that the 2-NBDG puncta appeared to be membrane-delimited (Supplemental Figure 2B). Arresting endosome maturation with a VPS34 inhibitor, VPS34 IN1, caused an enlargement of early endosomes which emphasized that 2-NBDG puncta are membrane-encased, endocytosed cargo. These findings constitute reliable evidence of robust endocytic activity in HAMEC, which readily internalize 2-NBDG and other small molecular weight solutes in the medium, including SRB.

The above findings challenge the concept that 2-NBDG might be transported primarily by GLUTs into the cytosol, which we found to be the main route of [^{3}H]-2-DG uptake. Indeed, in contrast to the uptake of radioactive glucose, the uptake of 2-NBDG was unaffected by 20 μM BAY-876 such that 2-NBDG continued to present as puncta that colocalized with SRB. The net amount of fluorescence in endosomes was also unaffected by the inhibitor or by 30 mM glucose (Supplemental Figure 3, A and B), nor was the number of endosomes different in each case (Supplemental Figure 3C). In contrast, 1 mM 2-NBDG or 1 mM 6-NBDG sufficed to reduce uptake of 50 μM [^{3}H]-2-DG by about 40% (Supplemental Figure 3D), similar to the potency of 1 mM 2-DG or glucose (Figure 1B). These findings indicate that 2-NBDG enters HAMEC through an endosomal route independent of facilitative glucose transporters, but 2-NBDG can inhibit these transporters, possibly through binding via its glucose moiety to the transporter without productive ligand turnover by the transporters into the cytosol.

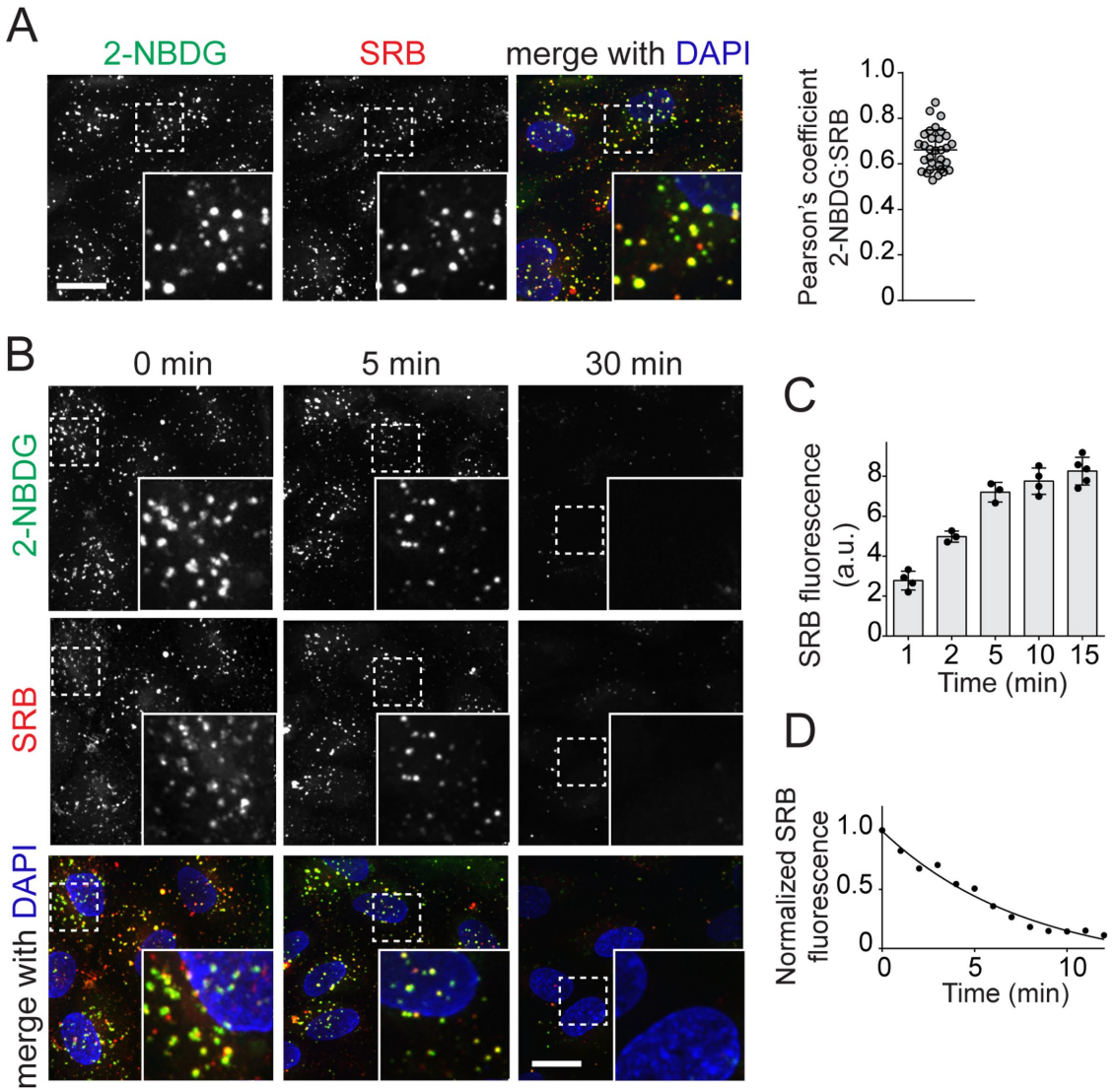

FIGURE 5: 2-NBDG enters HAMEC by pinocytosis. HAMEC underwent simultaneous loading of (A) 2-NBDG (300 μM) with Sulforhodamine B (SRB, 50 μM) in ECM for 15 min at 37°C. Cells were washed and fixed with 1% PFA in PBS for 1 min immediately before imaging. Shown are representative fields of view with insets magnified ×2. Scale bar, 10 μm. The degree of colocalization of 2-NBDG with SRB was calculated by Pearson's coefficient analysis using Volocity 6.1.2 software (three independent experiments of 10 fields, each containing 3–5 cells per experiment; bars represent mean ± SD). (B) HAMEC were pulsed with 2-NBDG and SRB (300 and 50 μM, respectively), rinsed to remove reagents, and then imaged by live-cell microscopy for 5 or 30 min at 37°C. Scale bar, 20 μm. (C) Time course of SRB uptake: HAMEC were pulsed for 1, 2, 5, 10, or 15 min with SRB (50 μM). SRB fluorescence was immediately acquired in independent fields of view using Volocity 6.1.2 software and is expressed as the mean ± SD fluorescence (a. u.) of three independent experiments of >15 cells per experiment. (D) Time course of SRB efflux: HAMEC were pulsed as in B and chased for 10 min, with fluorescence being recorded after each minute in independent fields of view. SRB fluorescence was normalized to the number of SRB-positive puncta before the chase period. Graphed are results from one representative of 3 independent experiments.

Endosomal recycling of 2-NBDG and Sulforhodamine B: implications for glucose uptake and release

Despite clear limitations of using 2-NBDG as an indicator of glucose transport in HAMEC, our imaging illuminated the underappreciated process of bulk nutrient uptake in endothelial cells by endocytosis/pinocytosis. Should endocytosed glucose be recycled to the basolateral surface of the cells, for example, via transendothelial vesicular transport, this could be an additional route of glucose transport across the endothelial barrier. Accordingly, we explored whether endosomes recycle their fluid-phase contents back into the solution in HAMEC. Following a 15-min pulse of 2-NBDG along with SRB, the cells were imaged over a subsequent 30 min period of chase (after removal of extracellular 2-NBDG and SRB). Because of the susceptibility of 2-NBDG to photobleaching, imaging at each point involved a separate field. Already after 5-min of chase, the number of 2-NBDG and SRB puncta was reduced, effectively disappearing by 30 min (Figure 5B).

Because of probe stability over time, SRB was used for a more detailed analysis of the rates of endocytic uptake and release. First, SRB uptake peaked by 15 min, when the steady-state fluorescence per cell stabilized (Figure 5C). The outlining of cell membranes with WGA–Alexa Fluor 647 conjugate confirmed that SRB staining is

within the cells (Supplemental Figure 2A). Confirming the dynamic endosomal recycling, chasing SRB fluorescence following the 15-min uptake pulse resulted in rapid SRB disappearance (Figure 5D). By 10 min of chase, virtually all SRB was released from the cells. These observations document the rapid uptake and release of endocytic fluid (with a $t_{½}$ of ~3 min for both formation and emptying), which result in the establishment of a steady state volume in the endocytic pathway. While this volume represents a small fraction compared with that of the cytosol, the rapid recycling of endocytic fluid suggests that a large amount of fluid passes through these endothelial cells.

A hallmark of endocytic recycling is the fusion of vesicles with the plasma membrane. The canonical fusogenic machinery involved, SNAREs, requires the ATPase N-ethylmaleimide–sensitive factor (NSF) for completion of the fusion cycle and, as its name indicates, NSF is highly susceptible to inhibition by N-ethylmaleimide (NEM). Accordingly, the acute inhibition by NEM is considered to be indicative of the participation of a vesicle–membrane fusion event in the process being interrogated (Wickner and Schekman, 2008). Following a 15-min pulse with SRB and 2-NBDG, the addition of 10 μM NEM during the chase period (15 min) stalled the release of SRB (Figure 6A) and 2-NBDG (Figure 6B). The results, calculated in Figure 6C, evince more than a 75% inhibition in fluid recycling. In stark contrast, NEM had no effect on the release of [^{3}H]-2-DG pulsed and chased under the same conditions (Figure 6D). Taken together, these findings suggest that while endocytosis does not exclude the uptake of glucose-sized molecules from the fluid, vesicle fusion is unlikely to contribute significantly to the measurements of [^{3}H]-2-DG release as indicated by the lack of inhibition of release by NEM. Accordingly, any endosome-trapped [^{3}H]-2-DG (and by extension, glucose) would conceivably traverse through endosomal membranes into the cytosol, possibly via GLUT1 (illustrated in Figure 7).

DISCUSSION

Circulating glucose crosses the endothelia of capillaries to reach parenchymal cells. While a transcellular route of glucose transit is required to overcome an endothelial barrier in most tissues, the molecular mechanisms whereby endothelial cells handle glucose and its delivery are poorly understood. That a significant kinetic barrier is indeed presented for the passive diffusion of glucose to tissues in vivo was established by continuous glucose monitoring of arterial blood and interstitial tissues by Nielsen *et al.* (2005). This study demonstrated a delay of ~20 min between the spike in glucose detected in arterial blood immediately after an injection of a bolus of glucose and the increase in glucose in adipose tissues, muscle or the central nervous system. On the other hand, it is also increasingly acknowledged that endothelial cells are highly glycolytic and that glucose metabolism is particularly important for genesis of the vasculature during development (Veys *et al.*, 2020). Moreover, reduced glucose metabolism of the endothelium features in pathological settings including in Alzheimer's disease (Furtado *et al.*, 2018). Clearly, the controlled balance between the use of glucose as an energy source and the flux of glucose by endothelial cells is an important physiology worthy of investigation.

Glucose transporters and glucose derivatives

We report that HAMEC, primary cells that preserve many of their in vivo morphological and phenotypic characteristics (Jaldin-Fincati *et al.*, 2018), express glucose transporters of the SLC2A family of facilitative hexose transporters. HAMEC were found to express predominantly express GLUT1 and GLUT3, which has also been observed for endothelial cells of coronary (Gaudreault *et al.*, 2008), umbilical vein and microdermal vessel origin (Tumova *et al.*, 2016). GLUT1 is also abundantly expressed in endothelial cells of brain, aorta, and adrenal microvessels (Gaposchkin and Garcia-Diaz, 1996). The use of radioactive and fluorescent glucose derivatives of glucose allowed us to identify uptake via these transporters as well as a dynamic uptake via endocytosis. We estimate that the major route for glucose uptake would be via glucose transporters, entering the cytosol where glucose is metabolically processed by phosphorylation and a fraction is incorporated into glycogen. This fraction is amenable for glycogenolysis and dephosphorylation, providing free glucose for export out of the cells. Our findings reveal two previously unrealized mechanisms protecting glucose from metabolic utilization by quiescent endothelial cells: glycogen accumulation and transient endosome trapping. Moreover, they identify the ability of microvascular endothelial cells to export glucose, which in an in vivo setting may contribute to the provision of glucose to parenchymal cells.

Isotopically labeled forms of 2-DG (with ^{3}H, ^{14}C, or ^{18}F) have been highly instrumental in measuring rates and routes of glucose uptake into cell populations. The fluorescent glucose derivative 2-NBDG has also been used to estimate glucose uptake in cell populations and in individual cells using cell sorting strategies, but surprisingly, its potential to discern the intracellular localization of glucose by fluorescence imaging has not been exploited. Both [^{3}H]-2-DG and 2-NBDG can be phosphorylated by hexokinases at position C-6 on the glucose molecule (generating [^{3}H]-2-DG-6-phosphate and 2-NBDG-6-phosphate) but cannot progress further to glycolysis, and though largely ignored, both are amenable to dephosphorylation (as measured in bacteria; Yoshioka *et al.*, 1996a).

Processing of 2-DG in the cytosol

Our results indicate that about 80% of [^{3}H]-2-DG entering HAMEC becomes readily phosphorylated, presumably by hexokinase. [^{3}H]-2-DG-6-phosphate would be expected to accumulate because it cannot undergo glycolysis. Additionally, about 20% is in an unphosphorylated form and incorporated into glycogen (Figure 2). Indeed, these cells have measurable levels of glycogen, in the range of those present in human hepatoma cells. Heralding these results, King *et al.* (1983) had shown incorporation of [^{14}C]-glucose into glycogen in retinal endothelial cells. Our findings corroborate that [^{3}H]-2-DG enters the HAMEC cytosol, where it becomes exposed to cytosolic enzymes. While most studies ignore the viability of 2-DG for metabolic incorporation into glycogen, this behavior is well documented. This would entail *bis*-phosphorylation to generate 2-deoxyglucose-1,6-bisphosphate and subsequently UDP-2-deoxyglucose. Measurements in vivo show that rate of glycogen synthesis from [^{3}H]-2-DG was rather identical to that for [U-^{14}C]-glucose, in most tissues (Pentreath *et al.*, 1982; Colwell *et al.*, 1996).

Human adipose tissue–derived microvascular endothelial cells mediate 2-DG efflux, involving 2-DG-phosphate dephosphorylation

A key finding of our study is that [^{3}H]-2-DG within HAMEC is not static, but rather a fraction is available for efflux. We found that 15–20% of the [^{3}H]-2-DG exits the cell within 30 min and continues to exit steadily. Our accounting of [^{3}H]-2-DG phosphorylation argues that the intracellular phosphorylated [^{3}H]-2-DG pool is the source for the efflux of unphosphorylated [^{3}H]-2-DG. Conceivably, this occurs through either direct action of the glucose-6-translocase/phosphatase complex at the membrane of the ER and/or through continuous glycogenolysis producing [^{3}H]-2-DG-6-phosphate. Both scenarios are buttressed by the reduction in [^{3}H]-2-DG efflux upon inhibition of the glucose-6-phosphate translocase or

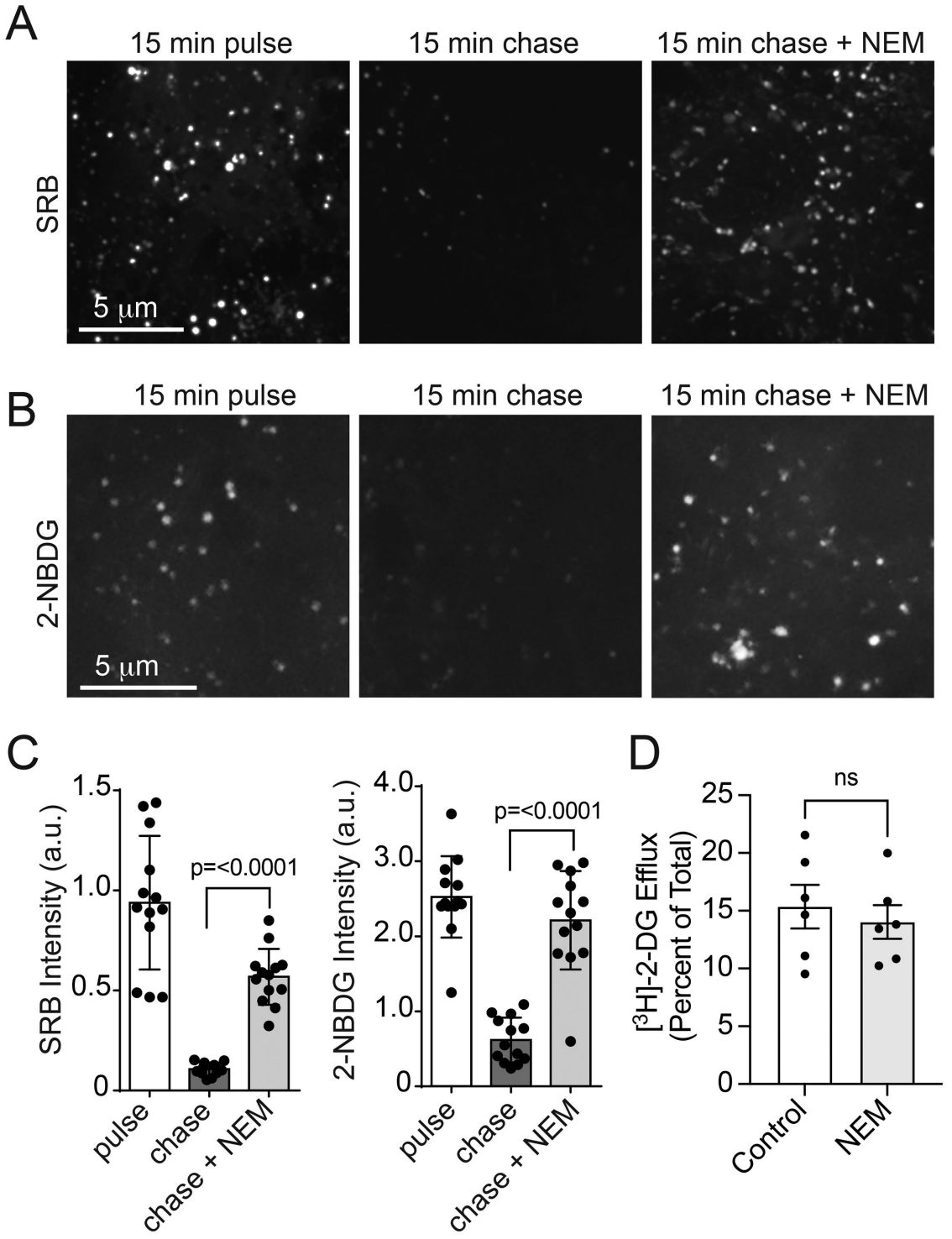

FIGURE 6: NEM prevents 2-NBDG and SRB recycling but not [^{3}H]-2-DG efflux. HAMEC were pulsed for 15 min with (A) SRB (50 μM) or (B) 2-NBDG (300 μM), rinsed and chased without SRB or 2-NBDG present in the absence or presence of 10 μM NEM. Shown are representative live-cell images during the pulse and chase periods with or without NEM. (C) Data represent >15 fields of 3–5 cells from three independent experiments. Bars represent the mean ± SD fluorescence (a. u.). (D) HAMEC were pulsed with [^{3}H]-2-DG (2 μCi/ml 50 μM, 30 min, 37°C). The cells were rinsed with PBS and chased in DMEM (with 5 mM glucose and FBS) for 30 min including 0.1% vol/vol DMSO (control) or 10 μM NEM. Efflux results are presented as the mean ± SEM percent [^{3}H]-counts released from the cells (relative to cell-associated [^{3}H]-counts in no-chase cells; $n = 6$ experiments, duplicate conditions; indicated p-value vs. control, Student's paired t test, two-tailed).

phosphatase functions. Moreover, the fact that adrenaline promoted [^{3}H]-2-DG efflux argues in favor of glycogenolysis also contributing [^{3}H]-2-DG-6-phosphate.

Free [^{3}H]-2-DG (or glucose) in the ER lumen must then become available for exit to the cytosol and out of the cell. Despite the long-recognized glycogenolytic and gluconeogenic activity of hepatocytes that produces the bulk of hepatic glucose output in vivo, the mechanism for glucose exit from the ER remains a 'black box' in the collective knowledge. This function was recently considered in view of advances in the detection of glucose transporters in this organelle. Lizak *et al.* (2019) hypothesized that glucose export from the ER lumen into the hepatocyte cytosol may be mediated by any or a combination of the following facilitated mechanisms: 1) transport via GLUT10, 2) transport via a non-GLUT family glucose transporter, 3) transport via newly synthesized GLUTs en route to the plasma membrane, or 4) transit via a non-selective translocon pore. The most compelling possibility is GLUT10, a member of the SLC2A family recently found to concentrate in the ER (Gamberucci *et al.*, 2017), to transport 2-deoxyglucose with a K_m of approximately 0.3 mM, and to be sensitive to inhibition by phloretin. Notably, other than the predominant GLUT1 and GLUT3 transcripts, HAMEC also express GLUT10. On the other hand, the use of glucose nanosensors targeted to the ER and cytosol of hepatoma cells suggested that a high-capacity, low-affinity, and cytochalasin B–insensitive mechanism mediates glucose liberated by the ER into the cytosol (Fehr *et al.*, 2005). Regardless of the molecular mechanism(s) involved, we envisage that glucose export from the ER must occur in regions closely apposed to the plasma membrane, in order to minimize rephosphorylation back to glucose-6-phosphate. Beyond these possibilities, it has also been hypothesized, in the case of hepatocytes and enterocytes, that ER-derived vesicles may empty directly into the extracellular milieu, accounting for some of the glycogenolytic and gluconeogenic glucose released by those cell types (Stumpel *et al.*, 2001).

In addition to generation of free glucose via glycogenolysis and export from the ER, glucose (or 2-deoxyglucose) incorporated into glycogen may also undergo glycophagy for content degradation by lysophagosomal glucosidases (Schneider *et al.*, 2014; Mandl and Banhegyi, 2018; Prats *et al.*, 2018). These particular lysophagosomes have been named glycophagosomes and should be able to release the glycogen hydrolysis products to the cytosol. Such release may be mediated by dedicated transporters at the delimiting membrane of this organelle (Lizak *et al.*, 2019). Indeed, recent studies point to GLUT6 (SLC2A6, earlier referred to as GLUT9; Lisinski *et al.*, 2001) as a lysosomal glucose transporter involved in glucose transport into the cytosol (Doege *et al.*, 2000). Compellingly, HAMEC express GLUT6, albeit at lower levels than GLUT1 and GLUT3.

Altogether, our study endorses the novel concept that glycogen depots in microvascular endothelial cells are dynamic, undergoing rapid glucose incorporation into glycogen, glycogenolysis and production of free glucose available for export out of the cell. An additional contribution by the autophagic pathway cannot be discounted and should be explored in future investigation.

Glucose efflux from the cytosol involves GLUT3

Ultimately, whether stemming from the phosphorylated pool, glycogenolysis, or autophagy, free glucose/2-DG released to the cytosol must readily exit the cells. The very minor reduction of efflux by 0.5 μM BAY-876, but more substantial inhibition at 20 μM, indicated that GLUT3 mediates about half of the efflux, with GLUT1 barely contributing to this function. Given that cytochalasin B caused a similar, partial inhibition of efflux, these results raise the possibility that an additional mechanism, likely not GLUT-mediated, participates in glucose efflux out of the cells. This additional mechanism remains to be fully investigated, with possibilities being 1) transport from the cytoplasm through other plasma membrane–based glucose transporters; 2) diffusion at ER sites that make contact with the plasma membrane; and 3) fusion of vesicles (originated from the ER or lysosome/glycophagosomes) with the plasma membrane.

Overall, our study highlights that GLUT1 and GLUT3 contribute equally to glucose entry into endothelial cells. Veys *et al.* (2020) have elegantly generated a mouse model for conditional knockout of GLUT1 in endothelial cells. Cells isolated from these mice had reduced glucose uptake compared with wild-type endothelial cells. Interestingly, GLUT1 expression increased as the cells in culture became quiescent cells while glycolysis was repressed, evincing that GLUT1 becomes uncoupled from glucose catabolism. Based on that study and our findings, we hypothesize that during angiogenesis or wound healing, GLUT1 mainly contributes to glycolysis, while in quiescent confluent cell monolayers, glucose uptake via GLUT1/3 is routed for exit from the cells and GLUT3 participates in this last step of glucose transcytosis.

Surprising differences between 2-DG and 2-NBDG uptake

Isotopically labeled forms of 2-DG (with 3H, 14C, or 18F) have been highly instrumental in measuring rates and routes of glucose uptake into cell populations. The fluorescent glucose derivative 2-NBDG has also been used to estimate glucose uptake in cell populations and in individual cells using cell sorting strategies, but surprisingly, its potential to discern the intracellular localization of glucose by fluorescence imaging has not been exploited.

Our study points out important differences in the behavior of 2-DG and 2-NBDG. Uptake of [^{3}H]-2-DG was inhibited by excess 2-DG, excess glucose, or the GLUT inhibitor BAY-876. The large differential susceptibility of GLUT1 and GLUT3 to inhibition by this drug allowed us to conclude that about 80% of uptake occurs through GLUTs, with GLUT1 and GLUT3 each mediating about half of the uptake at any time. In contrast, uptake of 2-NBDG was insensitive to these manipulations. We conclude that 2-NBDG is not taken up by HAMEC through GLUT1 or GLUT3, given 1) the discrete localization of the entering fluorescent glucose derivative in defined cytosolic puncta; 2) the insensitivity of 2-NBDG uptake to BAY-876 or high glucose, whether measured as number of puncta or net fluorescence intensity; 3) the clear demarcation of the 2-NBDG fluorescent puncta by plasma membrane-derived membrane, assigning them an endosomal identity; and 4) the behavior of the 2-NBDG puncta as recycling endosomes given their enlargement in cells treated with the endosomal PI-3-kinase inhibitor VPS34-IN1. Had 2-NBDG entered via membrane-associated transporters, a predominantly cytosolic distribution would have been expected. Indeed, this was the case of muscle cells overexpressing GLUT4 (Osorio-Fuentealba *et al.*, 2013) and tumor cells (O'Neil *et al.*, 2005), that generally have elevated expression of GLUT1.

These findings are consonant with recent reports that NBD-glucose analogues are not well-transported substrates of GLUT-family glucose transporters compared with glucose itself, challenging a body of prior literature attesting to their transport via these membrane proteins. For example, and most recently, CRISPR-Cas9 gene editing was used to ablate SLC2 (GLUTs), SLC5 (SGLTs), and SLC50 families of transporters in myeloma cells, yet 2-NBDG was still taken up unabated (D'Souza *et al.*, 2021). Two other recent studies dissociated the pharmacological sensitivity of 2-DG uptake and 2-NBDG uptake in T-cells and L929 cells (Sinclair *et al.*, 2020; Hamilton *et al.*, 2021). Of note, a major argument for considering 2-NBDG uptake is

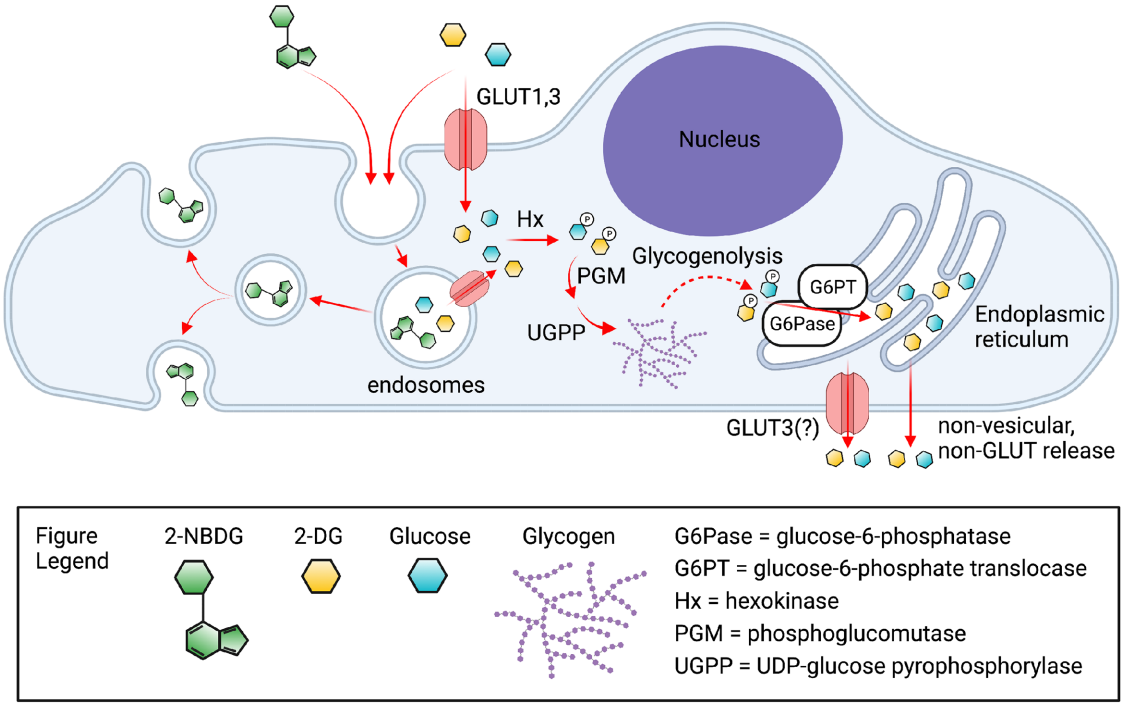

FIGURE 7: Schematic of the routes of uptake, intracellular processing, and efflux of 2-DG, 2-NBDG, and glucose. Uptake of 2-NBDG occurs via endocytosis and undergoes rapid recycling, given the inability of this glucose derivative to be transported via GLUT1 or GLUT3. In contrast, uptake of 2-DG reflects more faithfully the uptake of glucose and occurs primarily through GLUT1 and GLUT3, but it is also inferred to be taken up into endosomes via endocytosis. Given that the majority of 2-DG inside the cell becomes phosphorylated or incorporated into glycogen, it is inferred that the endosomal content of 2-DG (or glucose) must access the cytosol via endosomal transporters, mainly the abundant endosomal GLUT1. Phosphorylated 2-DG (or phosphorylated glucose), whether cytosolic or arising from glycogenolysis, is dephosphorylated by the ER-located glucose-6-phosphate translocase/phosphatase complex producing 2-DG (or glucose) in the ER lumen. Exit of 2-DG (or glucose) from the ER lumen is hypothesized to occur via GLUT10 by analogy to the case in liver, in close proximity to the plasma membrane. Final exit from the cells is mediated in part by GLUT3. Figure created using BioRender.com.

GLUT-mediated has been its sensitivity to high concentrations of cytochalasin B (Rudayni *et al.*, 2022), which in addition to its inhibitory actions on facilitative glucose transporters would reduce bulk fluid uptake via macropinocytosis due to its effects on the actin cytoskeleton. Indeed, we found that treatment of HAMEC with 10 μM cytochalasin B or performing uptake assays at 10°C equally and completely inhibited the uptake of both 2-NBDG and SRB (unpublished data).

Collectively, our findings reveal that 2-NBDG enters HAMEC largely via endocytosis and that at early times this cargo is readily recycled. These observations call for a cautionary note on studying 2-NBDG uptake and using cytochalasin B to determine participation of GLUTs; rather, imaging and acute inhibition by BAY-876 would be called for. On the other hand, 2-NBDG illuminated robust endocytic uptake and recycling activity in HAMEC. Because this process does not discriminate chemically among small molecules in the medium, 2-DG and glucose should be equally amenable to endocytosis. Interestingly, because [^{3}H]-2-DG efflux is not sensitive to NEM, whereas 2-NBDG release is, we surmise that the majority of [^{3}H]-2-DG (and glucose) would undergo extraction from the endocytosed fluid into the cytosol via GLUTs present on the endosomal membrane.

In conclusion, we describe mechanisms for uptake of glucose, its intracellular processing, and efflux mechanisms in microvascular endothelial cells. Our unanticipated findings reveal a major facilitative glucose transporter–mediated entry into the cytosol, and nondiscriminating small molecule uptake through endocytosis. Glucose entering the cytosol becomes readily phosphorylated and a significant fraction incorporates into glycogen. Both storage as glycogen and endocytic uptake constitute mechanisms escaping metabolic glucose utilization. Glycogen degradation and action of glucose-6-phosphatase generates free glucose that exits endothelial cells at least in part through facilitated glucose transporters. These mechanisms, illustrated in Figure 7, may contribute to transcellular glucose delivery across endothelia in vivo. We posit that, in addition to possible paracellular transport (not investigated here), glucose transfer to tissues, in vivo, involves endothelial cell uptake and release of glucose.

MATERIALS AND METHODS

Request a protocol through *Bio-protocol*.

Materials

2-Deoxy-D-[1,2-^{3}H(N)]-glucose (^{3}H2-DG) was from PerkinElmer (Cat. #NET549A, Santa Clara, CA, USA). 2-NBD glucose (2-NBDG or 2-(N-(7-Nitrobenz-2-oxa-1,3-diazol-4-yl)Amino)-2-Deoxy-glucose, Cat. #N13195), 6-NBDG (6-(N-(7-Nitrobenz-2-oxa-1,3-diazol-4-yl) amino)-6-Deoxy-glucose, Cat. #N23106), Sulforhodamine B (Cat #S1307), FM™4-64 Dye (N-(3-triethylammoniumpropyl)-4-(6-(4-(diethylamino) phenyl) hexatrienyl) pyridinium dibromide, Cat. #T3166), wheat germ agglutinin, Alexa Fluor 647 conjugate (Cat #W32466), DMEM with no glucose (Cat. #A1443001), and DAPI nucleic acid stain were from Thermo Fisher Scientific (Waltham, MA,

US). 2-Deoxy-D-glucose (Cat. #D8375), adrenaline (Cat. #E4375), BAY-876 (Cat. #SML1774) cytochalasin B (Cat. #C6762), Thielavin B (SMB00566), fibronectin (Cat #F1141), gelatin (Cat #G9391), anti-α-Actinin1 (Cat. #SAB4200813) were from Millipore-Sigma (Oakville, ON, Canada). VPS34-IN1 (Cat #S7980, Selleckchem, Houston, TX, USA). Anti-GLUT1 (Cat. #ab115730; Abcam PLC, Cambridge, MA, USA), anti-GLUT3 was a gift from Ian A. Simpson (Maher *et al*., 1992) and species-specific secondary antibodies conjugated with IRDye 800CW and IRDye 680LT (LI-COR, Lincoln, NE, USA) were used for immunoblotting. The inhibitor of glucose-6-phosphate translocase, S4048 (van Dijk *et al*., 2001), was obtained under MTA from Sanofi-Aventis Deutschland, GmbH with the assistance of Matthias Urmann.

TaqMan gene expression assays (FAM-MGB) for SLC2A1 (Hs00892681_m1), SLC2A2 (Hs01096908_m1), SLC2A3 (Hs00359840_m1), SLC2A4 (Hs00168966_m1), SLC2A5 (Hs01086390_m1), SLC2A6 (Hs00214042_m1), SLC2A7 (Hs01013558_m1), SLC2A8 (Hs00205863_m1), SLC2A9 (Hs01119178_m1), SLC2A10 (Hs05057221_s1), SLC2A11 (Hs00368843_m1), SLC2A12 (Hs00376943_m1), SLC5A1 (Hs01573793_m1), SLC5A2 (Hs00894942_m1), GYS1 (Hs00157863_m1), PYGM (Hs00989942_m1), PYGB (Hs00765686_m1), PYGL (Hs00958087_m1), G6PC (Hs02560787_s1), G6PC3 (Hs00978994_g1), and as the reference, ABT1 (Hs00706003_s1, VIC-MGB-PL), were from ThermoFisher Scientific (Waltham, MA, USA).

Human GLUT1-HA-HaloTag and GLUT3-HaloTag, with C-terminal fusion of the haloalkane dehalogenase HaloTag enzyme, were constructed as follows. The HaloTag enzyme was cloned into pCDNA3.1 and was a gift from Neil Goldenberg (The Hospital for Sick Children, Toronto, Canada). GLUT1-HA (human GLUT1 cDNA with an HA epitope tag in the first extracellular loop) was a previous gift from Dr. Al-Hasani (The German Diabetes Center [DDZ], University Düsseldorf, Germany; Al-Hasani *et al*., 1999). Human GLUT3 cDNA was subcloned from pDONR223_SLC2A3_WT (Cat# 81787, Addgene, Watertown, MA, USA). PCR reactions were performed using CloneAmp HiFi PCR Premix (Cat #639298, TakaraBio, San Jose, CA, USA). Primers to amplify GLUT1- HA were forward: 5′ccc aag ctg atg gag ccc agc agc aa 3′and reverse: 5′ttc tgc cat cac ttg gga atc agc cc 3′. Primers to amplify the HaloTag vector to accommodate GLUT1-HA were forward: 5′tcc caa gtg atg gca gaa atc ggt act g 3′ and reverse: 5′ggg ctc cat cag ctt ggg tct ccc tat a 3′. Primers to amplify GLUT3 were forward: ccc aag ctg atg ggg aca cag aag gtc a 3′and reverse: 5′ ttc tgc cat gac att ggt ggt ggt ctc 3′. Primers to amplify the HaloTag vector to accommodate GLUT3 were forward: 5′ acc aat gtc atg gca gaa atc ggt act g 3′ and reverse: 5′ tgt ccc cat cag ctt ggg tct ccc tat a 3′. PCR reaction products were cleaned using the NucleoSpin PCR Clean-up kit (Cat# 740609.10, Macherey-Nagel brand, distributed by Cedarlane, Burlington, Canada). PCR product fusions of 18bp overlapping regions between the pcDNA3.1 HaloTag vector and GLUT1-HA or GLUT3 were performed using the In-Fusion Snap Assembly EcoDry Master Mix (Cat#638954, Takarabio, USA). DNA sequencing using the CMV-fwd and BGH-rev primers confirmed in-frame insertions of GLUT1-HA and GLUT3 into the pCDNA3.1 HaloTag.

Cell culture

Primary human adipose microvascular endothelial cells (HAMEC; Cat. #7200; ScienCell, Carlsbad, CA, USA) were cultured in Endothelial Cell Medium kit (containing ECM, Cat. #1001prf; FBS, Cat #0025 and endothelial cell growth supplement [ECGS] Cat #1052 from ScienCell) in a humidified incubator at 37°C and 5% CO_2. Cells (passages 3–9) were grown in flasks coated with 2 μg/cm^2 fibronectin. For experimentation, cells were seeded in ECM plus supplements onto plates or coverslips precoated with 0.1% (wt/vol) gelatin in PBS containing Ca^{2+} and Mg^{2+} (PBS) and used by 48 h after reaching confluency (Jaldin-Fincati *et al*., 2018). The human liver cancer cell line Huh-7 was kindly provided by Anand Ghanekar (Toronto General Hospital Research Institute, Toronto, Canada). The cells were cultured with Life Technologies products (ThermoFisher Scientific, Waltham, MA, USA) Minimum Essential Medium (Cat. #10370021), supplemented with 0.01M HEPES buffer (Cat. #15630080), 1 mM sodium pyruvate (Cat. #11360070) and GlutaMAX (Cat. #35050061), Wisent Bio-Products (St. Bruno, QC, Canada), 100 U/ml penicillin/100 g/ml streptomycin (Cat # 450-200-EL), and 10% fetal bovine serum (Cat # 080-150).

[^{3}H]-2-DG uptake

This protocol was based on an earlier report with modifications (Rudich *et al*., 2003). Briefly, HAMEC confluent monolayers in 12-well plates were preincubated with inhibitors or vehicle in ECM without supplements for 5 min, washed with phosphate-buffered saline (PBS), and pulsed with 0.35 μCi/ 350 μl of [^{3}H]-2-DG (plus 50 μM nonradiolabeled 2-DG) in DMEM without glucose for 30 min (or the indicated times) at 37°C, followed by three washes with ice-cold PBS. Cells were lysed in 0.05 M NaOH and cell-associated radioactivity measured by scintillation counting in 5 ml Biosafe II complete counting cocktail (Cat #111195, RPI Corp.). Protein determinations were made (Bio-Rad protein assay Cat #5000006. Results were calculated as a percentage of the cell-associated radioactivity measured in the control or as nmol/mg protein versus time.

[^{3}H]-2-DG release

HAMEC confluent monolayers grown in six-well plates were washed with PBS and pulsed with 2 μCi/1.0 ml of [^{3}H]-2-DG (plus 50 μM nonradiolabeled 2-DG) in DMEM without glucose for 30 min at 37°C. This was followed by three washes with PBS at room temperature and immediately incubated in 1 ml DMEM with 5 mM glucose and 10% FBS for 0, 15, 30 min (or the chase time indicated) at 37°C. Reagents studied for effects on glucose release were added during the chase period only. Extracellular medium (1 ml) was collected before (0 min, background) or after the various chase times, and the corresponding cell monolayers, lysed in 0.05 M NaOH, for immediate scintillation counting. Results were calculated as a percentage of the total radioactivity recovered (cell lysate + media minus background) or as nmol released into the media/mg protein of cell lysate versus time.

Separation of [^{3}H]-2-DG and [^{3}H]-2-DG-phosphate

Cells grown in six-well plates were pulsed for 30 min with 2 μCi/ml [^{3}H]-2-DG, 50 μM 2-DG) in DMEM without glucose at 37°C. For the chase period, cells were incubated in 1 ml DMEM with 5 mM glucose and 10% FBS for 30 min. Aliquots of media (1 ml) were reserved, and cells were lysed with 50% ethanol and processed for ion exchange chromatography as described earlier (Konrad *et al*., 2005). In detail, lysates (intracellular) or media (extracellular) were processed separately, first by centrifugation for 15 min at 10,000 × *g*, 4°C, and aliquots (0.8 ml) were mixed with 0.2 ml of distilled-deionized water and loaded at 1 ml/min onto 1 ml Hi-Trap DEAE-FF columns (GE Healthcare Life Sciences, 17-5055-01) preequilibrated with five column volumes of distilled deionized 0.2 μm–filtered water. The flow-through was reloaded twice to ensure maximal binding of phosphorylated 2-DG to the DEAE anion exchanger and then reserved. The columns were washed with three successive 1-ml aliquots of 50 mM D-glucose and each flow-through aliquot was reserved. The columns were eluted with three successive 1-ml aliquots

of 200 mM HCl to displace the bound phosphorylated 2-DG and each flow-through aliquot was reserved. Radioactivity associated with 0.8-ml aliquots of each column flow-through (seven in total) was determined by liquid scintillation counting. Nonphosphorylated [^{3}H]-2-DG was calculated as the sum of [^{3}H]-dpm in the flow-through after sample loading plus the three glucose-wash flow-through aliquots, while phosphorylated [^{3}H]-2-DG was calculated as the sum of [^{3}H]-dpm in the three HCl eluted flow-through fractions. Results were calculated as the percentage nonphosphorylated or phosphorylated 2-DG relative to the total radioactivity recovered from all column fractions per sample.

[^{3}H]-2-DG incorporation into glycogen

Glycogen isolation was based on Carroll *et al.* (1956). Cells grown in 10-cm dishes were pulsed 2 µCi/ml [^{3}H]-2-DG (50 µM) in glucose-free DMEM for 30 min at 37°C. Cells were collected by scraping into PBS on ice, centrifuged at 800 × *g* for 5 min, and pellets were lysed in 600 µl of 30% wt/vol KOH saturated with Na_2SO_4. A 60-µl aliquot was reserved for [^{3}H]-counting. The remaining lysate was boiled for 20 min in screw-cap tubes. Lysates were cooled (4°C), mixed with 1.2 volumes of 95% ethanol (~660 µl), and incubated on ice for 10 min followed by centrifugation for 15 min at 10,000 × *g* for 4°C. The KOH/ethanol supernatants were reserved (soluble fraction) for [^{3}H] scintillation counting, and the pellets (containing glycogen) were washed twice by suspension in 1 ml of 95% ethanol and recentrifugation at 4°C. The glycogen pellets were easily dissolved in 1 ml of deionized–distilled water. These solubilized pellets were recentrifuged and the supernatants retained (glycogen fraction). Radioactivity associated with the suspended glycogen pellets was quantified by scintillation counting. Results are presented as the percentage of [^{3}H]-dpm associated with the KOH/ethanol supernatant or the solubilized glycogen pellet relative to the total radioactivity recovered from the original cell pellet.

Total cellular glycogen quantification

HAMEC and Huh-7 cellular glycogen content was determined using a colorimetric assay kit (ab169558, Abcam). Typically, 10^6 cells were pelleted, boiled in 200 µl of water for 10 min, homogenized, and processed according to kit instructions.

Gene expression analysis by RT-qPCR

RNA was purified using TRIzol and cDNA was synthesized using the SuperScript VILO cDNA kit (ThermoFisher Scientific, Waltham, MA, USA). RT-qPCR samples contained 10 ng of cDNA, Fast Advanced master mix, and predesigned TaqMan assays (containing FAM-MGB target gene probes), plus the primer-limited VIC-MGB reference gene probe. RT-qPCR was performed on Microamp 96-well Fast Optical reaction plate with an Applied Biosystems StepOnePlus system for 40 cycles (95°C for 1 s, 60°C for 20 s). Relative quantities of each mRNA were calculated using the comparative $\Delta\Delta C_T$ method with ABT1 expression as reference gene. For additional details, see Pillon *et al.* (2015).

Immunoblotting

Cells were rinsed with cold PBS and lysates collected in ice-cold lysis buffer (50 mM Tris, 150 mM NaCl, 1% Nonidet P-40, 0.5% sodium deoxycholate, 0.1% SDS) supplemented with 5 mM NaF, 1 mM EDTA, 1 mM PMSF, 5 mM Na_3VO_4. and protease inhibitors (P3840; Sigma-Aldrich). Twenty or fifty micrograms of protein were subjected to SDS–PAGE using 8–12% polyacrylamide gels. Proteins were transferred onto nitrocellulose membranes and blocked for 1 h with LI-COR blocking buffer and incubated overnight with primary antibodies in 1% BSA-TBST (Tris-buffered saline with Tween 20) at 4°C. Membranes were then incubated with fluorescent secondary antibodies for 45 min at room temperature and developed using an Odyssey Fc Imager (LI-COR). Results were quantified using Image Studio 4.0 software (LI-COR). For additional details, see Pillon *et al.* (2015).

Electroporation of HaloTag constructs of GLUT1 and GLUT3 and HaloTag detection

The cDNA constructs described above were introduced into HA-MEC using the Neon Electroporation transfection system (ThermoFisher Scientific Waltham, MA, USA). Cells were dislodged by trypsin treatment, collected in growth medium, and washed in PBS by centrifugation at 400 × *g* for 5 min. The pellets were suspended in Buffer R to 1.0×10^7 cells/ ml and 100 µl were mixed with 1.0 µg of either GLUT1-HA-HaloTag or GLUT3-HaloTag constructs and electroporated within the 100-µl tip (MPK10025 kit) according to a Neon-supported protocol for human microvascular endothelial cells, using 1150 V, 30 ms pulse width and two pulses. The electroporated cells were dispensed into two wells of a 12-well plate containing glass coverslips endothelial growth media and grown for 24 h. For fluorescent labeling of the fusion proteins, a 5X HaloTag working stock solution of Janelia Flour (JF)-549 HaloTag ligand (Cat #GA1110, Promega, Madison, WI, USA) was prepared in warm medium (1:200 dilution of master stock suspended in DMSO) just before addition to the cells at 37°C for 30 min in a humidified incubator with 5% CO_2. The cells were washed with PBS and fixed with 4% PFA for 10 min on ice and 10 min at room temperature before imaging by spinning disk confocal microscopy.

Fluorescent probes for imaging

HAMEC were grown on coverslips in ECM plus supplements to >80% confluency and pretreatment with competitors or inhibitors was performed for 5 min. The cells were then incubated in ECM (without serum and growth supplements) with 2-NBDG or 6-NBDG (300 µM) for 15 min at 37°C alone or in combination with competitors or inhibitors. For experiments with defined endpoints, coverslips were rinsed three times with PBS and fixed with 1% PFA in PBS for 1 min, and then mounted in Chamlide CMB magnetic imaging chambers (Quorum Technologies, Guelph, ON, Canada) in the fixative before imaging. For live-cell measurements of 2-NBDG (300 µM) and SRB (50 µM) recycling, cells were switched to warmed (37°C) Hank's balanced salt solution (HBSS) containing 2 mM glucose in imaging chambers and imaged at the indicated time points. To visualize membrane localization, FM 4-64 (1 µM) was added 5 min before 2-NBDG uptake and maintained during the uptake. The cells were then washed 3–4 times with cold HBSS and mounted in imaging chambers. WGA Alexa Fluor 647 conjugate was added at 1:1000 dilution for 1 min before imaging in cold PBS.

Live-cell confocal fluorescence microscopy and analysis

Fluorescence images in live-cells were captured with a 60 × 1.35 numerical aperture (NA) oil immersion objective using an Olympus IX81 Quorum spinning-disk confocal microscope. The microscope was equipped with a CSU-X1-A Yokogawa spinning-disk unit and a Hamamatsu C9100-13 EM-CCD camera controlled by Volocity 6.1.2 software (PerkinElmer, Santa Clara, CA, USA). For NBD imaging, samples were excited at 488 nm and fluorescence captured at 505–550 nm bandpass filter emission. Fluorescent images shown as volume-render projections belong to *Z*-stacks acquired at 0.4 µm. Image colocalization analysis was performed using Pearson's correlation analysis with Volocity 6.1.2 software.

Statistical analysis

Analyses were performed using Prism 9.0 software (GraphPad Software, San Diego, CA) and all experiments were performed at least three times unless indicated, with various internal replicates depending on the assay. For live cell imaging analysis, at least a total of 100 cells were included. Statistical differences between two groups of data were analyzed by Student's *t* test. One-way ANOVA was used to test differences between groups with equal variances. Statistical significance was set at $p < 0.05$. Data were expressed as mean ± SEM or SD.

ACKNOWLEDGMENTS

We thank Anand Ghanekar (Toronto General Hospital Research Institute, Canada) for the Huh7 human liver cancer cell line; Matthias Urmann for facilitating transfer of S4048 from Sanofi-Aventis Deutschland; and Ian Simpson for anti-GLUT3. We thank Neil Goldenberg for providing pcDNA3.1 HaloTag, Allen Volchuk and Zhi Liu for creating the GLUT1-HA HaloTag and GLUT3 HaloTag plasmids, and the latter for further technical support. We sincerely thank the late Peter Roach for helpful advice, as well as Victoria Tokarz, Scott Frendo-Cumbo, and Cesar Osorio-Fuentealba for useful discussion. This work was supported by a Foundation Grant to A.K. (FDN-143203) from the Canadian Institutes of Health Research (CIHR) and by a Project Grant (PJT-169180) from CIHR to S.A.F. Personnel support from a Canada Research Chair Tier II to S.A.F., from a Diabetes Canada Postdoctoral fellowship (PF-3-17-5308-SY) to S.Y., from a Lymphatic Education and Research Network and Fat Disorders Research Society (LE&RN/FDRS) postdoctoral Fellowship to J.J-F., and from the SSuRe and Lunenfeld Summer Programs to J.P., F.C., and E.S. is acknowledged.

REFERENCES

Al-Hasani H, Yver DR, Cushman SW (1999). Overexpression of the glucose transporter GLUT4 in adipose cells interferes with insulin-stimulated translocation. FEBS Lett 460, 338–342.

Azizi PM, Zyla RE, Guan S, Wang C, Liu J, Bolz SS, Heit B, Klip A, Lee WL (2015). Clathrin-dependent entry and vesicle-mediated exocytosis define insulin transcytosis across microvascular endothelial cells. Mol Biol Cell 26, 740–750.

Bandsma RH, Wiegman CH, Herling AW, Burger HJ, ter Harmsel A, Meijer AJ, Romijn JA, Reijngoud DJ, Kuipers F (2001). Acute inhibition of glucose-6-phosphate translocator activity leads to increased de novo lipogenesis and development of hepatic steatosis without affecting VLDL production in rats. Diabetes 50, 2591–2597.

Betz AL, Csejtey J, Goldstein GW (1979). Hexose transport and phosphorylation by capillaries isolated from rat brain. Am J Physiol 236, C96–C102.

Carroll NV, Longley RW, Roe JH (1956). The determination of glycogen in liver and muscle by use of anthrone reagent. J Biol Chem 220, 583– 593.

Colwell DR, Higgins JA, Denyer GS (1996). Incorporation of 2-deoxy-D-glucose into glycogen. Implications for measurement of tissue-specific glucose uptake and utilisation. Int J Biochem Cell Biol 28, 115–121.

D'Souza LJ, Wright SH, Bhattacharya D (2021). Genetic evidence that uptake of the fluorescent analog 2NBDG occurs independently of known glucose transporters. bioRxiv doi: https://doi.org/10.1101/2021.12.13.472409.

De Bock K, Georgiadou M, Carmeliet P (2013). Role of endothelial cell metabolism in vessel sprouting. Cell Metab 18, 634–647.

De Vivo DC, Trifiletti RR, Jacobson RI, Ronen GM, Behmand RA, Harik SI (1991). Defective glucose transport across the blood–brain barrier as a cause of persistent hypoglycorrhachia, seizures, and developmental delay. N Engl J Med 325, 703–709.

Doege H, Bocianski A, Joost HG, Schurmann A (2000). Activity and genomic organization of human glucose transporter 9 (GLUT9), a novel member of the family of sugar-transport facilitators predominantly expressed in brain and leucocytes. Biochem J 350(Pt 3), 771–776.

Fehr M, Takanaga H, Ehrhardt DW, Frommer WB (2005). Evidence for high-capacity bidirectional glucose transport across the endoplasmic reticulum membrane by genetically encoded fluorescence resonance energy transfer nanosensors. Mol Cell Biol 25, 11102–11112.

Furtado D, Bjornmalm M, Ayton S, Bush AI, Kempe K, Caruso F (2018). Overcoming the blood–brain barrier: the role of nanomaterials in treating neurological diseases. Adv Mater, e1801362.

Gamberucci A, Marcolongo P, Nemeth CE, Zoppi N, Szarka A, Chiarelli N, Hegedus T, Ritelli M, Carini G, Willaert A, *et al.* (2017). GLUT10-lacking in arterial tortuosity syndrome-is localized to the endoplasmic reticulum of human fibroblasts. Int J Mol Sci 18, 1820.

Gaposchkin CG, Garcia-Diaz JF (1996). Modulation of cultured brain, adrenal, and aortic endothelial cell glucose transport. Biochim Biophys Acta 1285, 255–266.

Gaudreault N, Scriven DR, Laher I, Moore ED (2008). Subcellular characterization of glucose uptake in coronary endothelial cells. Microvasc Res 75, 73–82.

Goldstein GW, Csejtey J, Diamond I (1977). Carrier mediated glucose transport in capillaries isolated from rat brain. J Neurochem 28, 725–728.

Gustafson LA, Neeft M, Reijngoud DJ, Kuipers F, Sauerwein HP, Romijn JA, Herling AW, Burger HJ, Meijer AJ (2001). Fatty acid and amino acid modulation of glucose cycling in isolated rat hepatocytes. Biochem J 358, 665–671.

Hamilton KE, Bouwer MF, Louters LL, Looyenga BD (2021). Cellular binding and uptake of fluorescent glucose analogs 2-NBDG and 6-NBDG occurs independent of membrane glucose transporters. Biochimie 190, 1–11.

Horton RW, Meldrum BS, Bachelard HS (1973). Enzymic and cerebral metabolic effects of 2-deoxy-D-glucose. J Neurochem 21, 507–520.

Huang Y, Lei L, Liu D, Jovin I, Russell R, Johnson RS, Di Lorenzo A, Giordano FJ (2012). Normal glucose uptake in the brain and heart requires an endothelial cell–specific HIF-1alpha-dependent function. Proc Natl Acad Sci USA 109, 17478–17483.

Jaldin-Fincati JR, Pereira RVS, Bilan PJ, Klip A (2018). Insulin uptake and action in microvascular endothelial cells of lymphatic and blood origin. Am J Physiol Endocrinol Metab 315, E204–E217.

King GL, Buzney SM, Kahn CR, Hetu N, Buchwald S, Macdonald SG, Rand LI (1983). Differential responsiveness to insulin of endothelial and support cells from micro- and macrovessels. J Clin Invest 71, 974–979.

Knott RM, Robertson M, Muckersie E, Forrester JV (1996). Regulation of glucose transporters (GLUT-1 and GLUT-3) in human retinal endothelial cells. Biochem J 318(Pt 1), 313–317.

Koepsell H (2020). Glucose transporters in brain in health and disease. Pflugers Arch 472, 1299–1343.

Konrad D, Rudich A, Bilan PJ, Patel N, Richardson C, Witters LA, Klip A (2005). Troglitazone causes acute mitochondrial membrane depolarisation and an AMPK-mediated increase in glucose phosphorylation in muscle cells. Diabetologia 48, 954–966.

Lisinski I, Schurmann A, Joost HG, Cushman SW, Al-Hasani H (2001). Targeting of GLUT6 (formerly GLUT9) and GLUT8 in rat adipose cells. Biochem J 358, 517–522.

Lizak B, Szarka A, Kim Y, Choi KS, Nemeth CE, Marcolongo P, Benedetti A, Banhegyi G, Margittai E (2019). Glucose transport and transporters in the endomembranes. Int J Mol Sci 20, 5898.

Los GV, Encell LP, McDougall MG, Hartzell DD, Karassina N, Zimprich C, Wood MG, Learish R, Ohana RF, Urh M, *et al.* (2008). HaloTag: a novel protein labeling technology for cell imaging and protein analysis. ACS Chem Biol 3, 373–382.

Maher F, Vannucci S, Takeda J, Simpson IA (1992). Expression of mouse-GLUT3 and human-GLUT3 glucose transporter proteins in brain. Biochem Biophys Res Commun 182, 703–711.

Mandl J, Banhegyi G (2018). The ER—glycogen particle—phagophore triangle: a hub connecting glycogenolysis and glycophagy? Pathol Oncol Res 24, 821–826.

Mueckler M, Thorens B (2013). The SLC2 (GLUT) family of membrane transporters. Mol Aspects Med 34, 121–138.

Nielsen JK, Djurhuus CB, Gravholt CH, Carus AC, Granild-Jensen J, Orskov H, Christiansen JS (2005). Continuous glucose monitoring in interstitial subcutaneous adipose tissue and skeletal muscle reflects excursions in cerebral cortex. Diabetes 54, 1635–1639.

Nigam VN (1967). Incorporation of 2-deoxyglucose into glycogen by intact Novikoff ascites hepatoma. Arch Biochem Biophys 120, 232–233.

Nigam VN, Fridland A (1967). Studies on glycogen synthesis in pigeon liver homogenates. Incorporation of hexose into glycogen. Biochem J 105, 505–513.

O'Neil RG, Wu L, Mullani N (2005). Uptake of a fluorescent deoxyglucose analog (2-NBDG) in tumor cells. Mol Imaging Biol 7, 388–392.

Osorio-Fuentealba C, Contreras-Ferrat AE, Altamirano F, Espinosa A, Li Q, Niu W, Lavandero S, Klip A, Jaimovich E (2013). Electrical stimuli release

ATP to increase GLUT4 translocation and glucose uptake via PI3K-gamma-Akt-AS160 in skeletal muscle cells. Diabetes 62, 1519–1526.
Patching SG (2017). Glucose transporters at the blood–brain barrier: function, regulation and gateways for drug delivery. Mol Neurobiol 54, 1046–1077.
Pentreath VW, Seal LH, Kai-Kai MA (1982). Incorporation of [3H]2-deoxyglucose into glycogen in nervous tissues. Neuroscience 7, 759–767.
Pillon NJ, Azizi PM, Li YE, Liu J, Wang C, Chan KL, Hopperton KE, Bazinet RP, Heit B, Bilan PJ, *et al.* (2015). Palmitate-induced inflammatory pathways in human adipose microvascular endothelial cells promote monocyte adhesion and impair insulin transcytosis. Am J Physiol Endocrinol Metab 309, E35–E44.
Prats C, Graham TE, Shearer J (2018). The dynamic life of the glycogen granule. J Biol Chem 293, 7089–7098.
Rohlenova K, Veys K, Miranda-Santos I, De Bock K, Carmeliet P (2018). Endothelial cell metabolism in health and disease. Trends Cell Biol 28, 224–236.
Rudayni HA, Stephenson G, Posterino GS (2022). Measurements of basal d-glucose transport through GLUT1 across the intact plasma membrane of isolated segments from single fast- and slow-twitch skeletal muscle fibres of rat. Acta Physiol (Oxf) 234, e13789.
Rudich A, Konrad D, Torok D, Ben-Romano R, Huang C, Niu W, Garg RR, Wijesekara N, Germinario RJ, Bilan PJ, Klip A (2003). Indinavir uncovers different contributions of GLUT4 and GLUT1 towards glucose uptake in muscle and fat cells and tissues. Diabetologia 46, 649–658.
Sakemi S, Hirai H, Ichiba T, Inagaki T, Kato Y, Kojima N, Nishida H, Parker JC, Saito T, Tonai-Kachi H, *et al.* (2002). Thielavins as glucose-6-phosphatase (G6Pase) inhibitors: producing strain, fermentation, isolation, structural elucidation and biological activities. J Antibiot (Tokyo) 55, 941–951.
Schneider JL, Suh Y, Cuervo AM (2014). Deficient chaperone-mediated autophagy in liver leads to metabolic dysregulation. Cell Metab 20, 417–432.
Siebeneicher H, Cleve A, Rehwinkel H, Neuhaus R, Heisler I, Muller T, Bauser M, Buchmann B (2016). Identification and optimization of the first highly selective GLUT1 inhibitor BAY-876. ChemMedChem 11, 2261–2271.
Sinclair LV, Barthelemy C, Cantrell DA (2020). Single cell glucose uptake assays: a cautionary tale. Immunometabolism 2, e200029.
Stumpel F, Burcelin R, Jungermann K, Thorens B (2001). Normal kinetics of intestinal glucose absorption in the absence of GLUT2: evidence for a transport pathway requiring glucose phosphorylation and transfer into the endoplasmic reticulum. Proc Natl Acad Sci USA 98, 11330–11335.
Szablewski L (2017). Glucose transporters in brain: in health and in Alzheimer's disease. J Alzheimers Dis 55, 1307–1320.
Tumova S, Kerimi A, Porter KE, Williamson G (2016). Transendothelial glucose transport is not restricted by extracellular hyperglycaemia. Vascul Pharmacol 87, 219–229.
van Dijk TH, van der Sluijs FH, Wiegman CH, Baller JF, Gustafson LA, Burger HJ, Herling AW, Kuipers F, Meijer AJ, Reijngoud DJ (2001). Acute inhibition of hepatic glucose-6-phosphatase does not affect gluconeogenesis but directs gluconeogenic flux toward glycogen in fasted rats. A pharmacological study with the chlorogenic acid derivative S4048. J Biol Chem 276, 25727–25735.
van Schaftingen E, Gerin I (2002). The glucose-6-phosphatase system. Biochem J 362, 513–532.
Veys K, Fan Z, Ghobrial M, Bouche A, Garcia-Caballero M, Vriens K, Conchinha NV, Seuwen A, Schlegel F, Gorski T, *et al.* (2020). Role of the GLUT1 glucose transporter in postnatal CNS angiogenesis and blood–brain barrier integrity. Circ Res 127, 466–482.
Virkamaki A, Rissanen E, Hamalainen S, Utriainen T, Yki-Jarvinen H (1997). Incorporation of [3-3H]glucose and 2-[1-14C]deoxyglucose into glycogen in heart and skeletal muscle in vivo: implications for the quantitation of tissue glucose uptake. Diabetes 46, 1106–1110.
Vorhaben JE, Campbell JW (1979). Subcellular localization of glucose-6-phosphatase in animal tissues. Comp Biochem Physiol B 62, 85–87.
Wickner W, Schekman R (2008). Membrane fusion. Nat Struct Mol Biol 15, 658–664.
Willemsen MA, Vissers LE, Verbeek MM, van Bon BW, Geuer S, Gilissen C, Klepper J, Kwint MP, Leen WG, Pennings M, *et al.* (2017). Upstream SLC2A1 translation initiation causes GLUT1 deficiency syndrome. Eur J Hum Genet 25, 771–774.
Yamada K, Nakata M, Horimoto N, Saito M, Matsuoka H, Inagaki N (2000). Measurement of glucose uptake and intracellular calcium concentration in single, living pancreatic beta-cells. J Biol Chem 275, 22278–22283.
Yamada K, Saito M, Matsuoka H, Inagaki N (2007). A real-time method of imaging glucose uptake in single, living mammalian cells. Nat Protoc 2, 753–762.
Yazdani S, Jaldin-Fincati JR, Pereira RVS, Klip A (2019). Endothelial cell barriers: Transport of molecules between blood and tissues. Traffic 20, 390–403.
Yoshioka K, Saito M, Oh KB, Nemoto Y, Matsuoka H, Natsume M, Abe H (1996a). Intracellular fate of 2-NBDG, a fluorescent probe for glucose uptake activity, in *Escherichia coli* cells. Biosci Biotechnol Biochem 60, 1899–1901.
Yoshioka K, Takahashi H, Homma T, Saito M, Oh KB, Nemoto Y, Matsuoka H (1996b). A novel fluorescent derivative of glucose applicable to the assessment of glucose uptake activity of *Escherichia coli*. Biochim Biophys Acta 1289, 5–9.